US010146029B2

(12) **United States Patent**
Hua et al.

(10) **Patent No.: US 10,146,029 B2**
(45) **Date of Patent: Dec. 4, 2018**

(54) **HEAD-MOUNTED PROJECTION DISPLAY USING REFLECTIVE MICRODISPLAYS**

(71) Applicant: **The Arizona Board of Regents on Behalf of the University of Arizona**, Tucson, AZ (US)

(72) Inventors: **Hong Hua**, Tucson, AZ (US); **Rui Zhang**, Kirkland, WA (US)

(73) Assignee: **THE ARIZONA BOARD OF REGENTS ON BEHALF OF THE UNIVERSITY OF ARIZONA**, Tucson, AZ (US)

(*) Notice: Subject to any disclaimer, the term of this patent is extended or adjusted under 35 U.S.C. 154(b) by 0 days.

(21) Appl. No.: **15/092,831**

(22) Filed: **Apr. 7, 2016**

(65) **Prior Publication Data**

US 2017/0059831 A1 Mar. 2, 2017

Related U.S. Application Data

(60) Continuation of application No. 13/955,076, filed on Jul. 31, 2013, now Pat. No. 9,310,591, which is a (Continued)

(51) **Int. Cl.**
G02B 13/22 (2006.01)
G02B 27/01 (2006.01)
(Continued)

(52) **U.S. Cl.**
CPC ***G02B 13/22*** (2013.01); ***G02B 5/3083*** (2013.01); ***G02B 13/004*** (2013.01); ***G02B 13/0065*** (2013.01); ***G02B 13/04*** (2013.01); ***G02B 13/16*** (2013.01); ***G02B 27/0172*** (2013.01); *G02B 5/30* (2013.01); *G02B 9/34* (2013.01); *G02B 27/286* (2013.01); *G02B 2027/0118* (2013.01); *G02B 2027/0123* (2013.01)

(58) **Field of Classification Search**
CPC .. G02B 13/22; G02B 27/0172; G02B 27/286; G02B 2027/0123; G02B 9/34; G02B 5/30
See application file for complete search history.

(56) **References Cited**

U.S. PATENT DOCUMENTS

3,632,184 A 1/1972 King
5,109,469 A 4/1992 Duggan
(Continued)

FOREIGN PATENT DOCUMENTS

EP 0408344 1/1991
EP 1102105 5/2001
(Continued)

OTHER PUBLICATIONS

US 9,880,387, 01/2018, Hua (withdrawn)
(Continued)

Primary Examiner — Tony Ko
(74) *Attorney, Agent, or Firm* — Niels Haun; Dann, Dorfman, Herrell & Skillman, P.C.

(57) **ABSTRACT**

The present invention relates generally to a head-mounted projection display, and more particularly, but not exclusively to a polarized head-mounted projection display including a light engine and a compact, high-performance projection lens for use with reflective microdisplays.

11 Claims, 17 Drawing Sheets

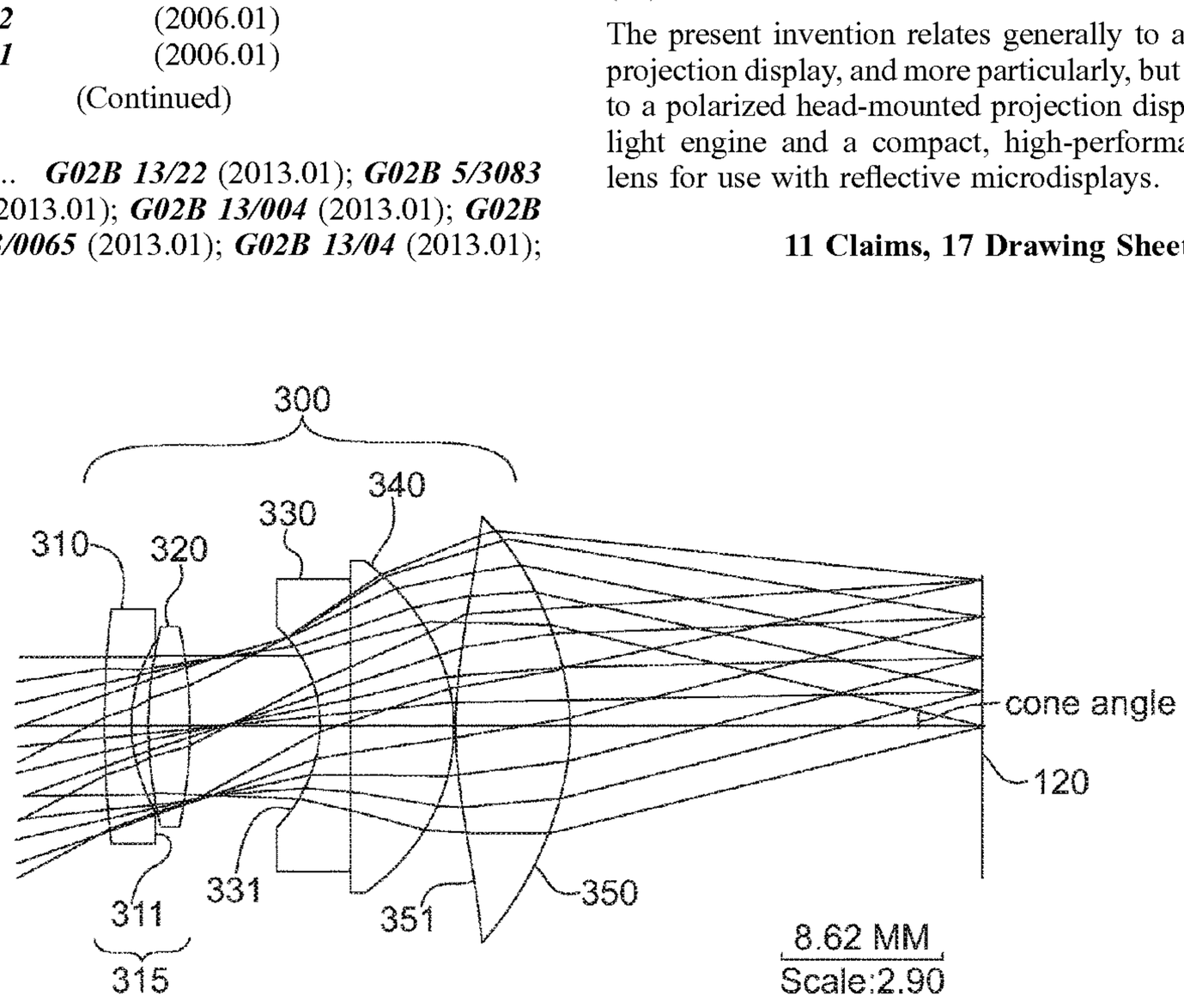

Related U.S. Application Data

division of application No. 12/863,771, filed as application No. PCT/US2009/031606 on Jan. 21, 2009, now Pat. No. 8,511,827.

(60) Provisional application No. 61/011,789, filed on Jan. 22, 2008.

(51) **Int. Cl.**

G02B 5/30	(2006.01)
G02B 13/00	(2006.01)
G02B 13/04	(2006.01)
G02B 13/16	(2006.01)
G02B 9/34	(2006.01)
G02B 27/28	(2006.01)

(56) **References Cited**

U.S. PATENT DOCUMENTS

5,436,763	A	7/1995	Chen	
6,008,781	A	12/1999	Furness	
6,239,915	B1	5/2001	Takagi	
6,646,811	B2	11/2003	Inoguchi	
6,653,989	B2	11/2003	Nakanishi	
7,405,881	B2	7/2008	Shimizu	
9,310,591	B2	4/2016	Hua	
9,874,760	B2	1/2018	Hua	
2002/0060850	A1	5/2002	Takeyama	
2002/0063913	A1	5/2002	Nakamura	
2004/0136097	A1	7/2004	Park	
2004/0218243	A1	11/2004	Yamazaki	
2004/0233551	A1	11/2004	Takahashi	
2005/0179868	A1	8/2005	Seo	
2008/0036853	A1	2/2008	Shestak	
2010/0091027	A1	4/2010	Oyama	
2010/0208372	A1*	8/2010	Heimer	G01J 3/02 359/834
2010/0271698	A1	10/2010	Kessler	
2010/0289970	A1	11/2010	Watanabe	
2012/0013988	A1	1/2012	Hutchin	
2012/0050891	A1	3/2012	Seidl	
2012/0242697	A1	9/2012	Border	
2013/0100524	A1	4/2013	Magarill	
2013/0222896	A1	8/2013	Komatsu	
2013/0285885	A1	10/2013	Nowatzyk	
2014/0300869	A1	10/2014	Hirsch	
2015/0168802	A1	6/2015	Bohn	
2015/0277129	A1	10/2015	Hua	
2015/0363978	A1	12/2015	Maimone	
2016/0085075	A1	3/2016	Cheng	
2016/0239985	A1	8/2016	Haddick et al.	
2016/0320620	A1	11/2016	Maimone	
2017/0202633	A1	7/2017	Liu	
2018/0045949	A1	2/2018	Hua	

FOREIGN PATENT DOCUMENTS

JP	H10307263	11/1998
JP	2003241100	8/2003
WO	2015134740	9/2015
WO	2016033317	3/2016
WO	2018052590	3/2018

OTHER PUBLICATIONS

H. Hua, P. Krishnaswamy, and J.P. Rolland, 'Video-based eyetracking methods and algorithms in head-mounted displays,' Opt. Express, 14(10):4328-50, May 2006.

H. Hua, Y. Ha, and J. P. Rolland, 'Design of an ultra-light and compact projection lens,' Appl. Opt. 42, 1-12 (2003), pp. 37-107.

H. Hua., A. Girardot, C. Gao. J. P. Rolland. 'Engineering of head-mounted projective displays'. Applied Optics. 39 (22), pp. 3814-3824. (2000).

H. Hua and C. Gao, "A polarized head-mounted projective display," in Proceedings of IEEE and ACM International Symposium on Mixed and Augmented Reality 2005 (IEEE, 2005), pp. 32-35.

Heanue et al., "Volume Holographic Storage and Retrieval of Digital Data," Science 265:749-752 (1994).

Hidenori Kuriyabashi, Munekazu Date, Shiro Suyama, Toyohiko HatadaJ. of the SID 14/5, 2006 pp. 493-498.

Hua, "Merging the Worlds of Atoms and Bits: Augmented Virtual Environments," Optics and Photonics News 17:26-33 (2006).

Hua, H., C. Pansing, and J. P. Rolland, "Modeling of an eye-imaging system for optimizing illumination schemes in an eye-tracked head-mounted display," Applied Optics, 46(32): 1-14, Nov. 2007.

Hua, H. "Integration of eye tracking capability into optical see-through head-mounted displays," Proceedings of SPIE (Electronic Imaging 2001), pp. 496-503, Jan. 2001.

Hua et al, "Compact eyetracked optical see-through head-mounted display", Proc. SPIE 8288, Stereoscopic Displays and Applications XXIII, 82881F (Feb. 9, 2012).

Hua et al., 'Design of a Bright Polarized Head-Mounted Projection Display' Applied Optics 46:2600-2610 (2007).

Inoue et al., "Accommodative Responses to Stereoscopic Three-Dimensional Display," Applied Optics, 36:4509-4515 (1997).

International Search Report and Written Opinion dated Nov. 24, 2015 in corresponding PCT application PCT/US2015/047163.

International Search Report dated Feb. 10, 2011 from PCT/CN2010/072376.

International Search Report dated Jan. 29, 2014 in corresponding international application PCT/US2013/065422.

International Search Report dated Jun. 18, 2010 in corresponding international application PCT/US2010/031799.

International Search Report dated Mar. 9, 2009 with regard to International Patent Application No. PCT/US2009/031606.

J. Hong, S. Min, and B. Lee, "Integral floating display systems for augmented reality," Applixed Optics, 51 (18):4201-9, 2012.

J. S. Jang and B. Javidi, "Large depth-of-focus time-multiplexed three-dimensional integral imaging by use of lenslets with non-uniform focal lengths and aperture sizes," Opt. Lett. vol. 28, pp. 1924-1926 (2003).

J. Arai, et al., "Depth-control method for integral imaging," Feb. 1, 2008 / vol. 33, No. 3 / Optics Letters.

J. E. Melzer's: 'Overcoming the field-of- view/resolution invariant in head-mounted displays' Proc. SPIE vol. 3362, 1998, p. 284.

J. G. Droessler, D. J. Rotier, "Tilted cat helmet-mounted display," Opt. Eng., vol. 29, 849 (1990).

J. L. Pezzaniti and R. A. Chipman, "Angular dependence of polarizing beam-splitter cubes," Appl. Opt. 33, 1916-1929 (1994).

J. P. Rolland, F. Biocca, F. Hamza-Lup, Y. Ha, and R. Martins, "Development of head-mounted projection displays for Distributed, collaborative, augmented reality applications," Presence: Teleoperators and Virtual Environments 14, 528-549 (2005).

J. P. Rolland, "Wide-angle, off-axis, see-through head-mounted display," Opt. Eng., vol. 39, 1760 (2000).

J. P. Rolland and Hong Hua. "Head-mounted display systems," in Encyclopedia of Optical Engineering. R. Barry Johnson and Ronald O. Driggers, Eds, (2005).

J. S. Jang, F. Jin, and B. Javidi, "Three-dimensional integral imaging with large depth of focus by use of real and virtual image fields," Opt. Lett. 28:1421-23, 2003.

J. Y. Son, W.H Son, S.K. Kim, K.H. Lee, B. Javidi, "Three-Dimensional Imaging for Creating Real-World-Like Environments," Proceedings of IEEE Journal, vol. 101, issue 1, pp. 190-205, Jan. 2013.

Jisoo Hong, et al., "Three-dimensional display technologies of recent interest: Principles, Status, and Issues," Applied Optics (Dec. 1, 2011) 50(34):106.

K. Iwamoto, K. Tanie, T. T. Maeda, "A head-mounted eye movement tracking display and its image display method", Systems & Computers in Japan, vol. 28, No. 7, Jun. 30, 1997, pp. 89-99. Publisher: Scripta Technica, USA.

K. Iwamoto, S. Katsumata, K. Tanie, "An eye movement tracking type head mounted display for virtual reality system: —evaluation experiments of a prototype system", Proceedings of 1994 IEEE International Conference on Systems, Man, and Cybernetics. Humans,

(56) **References Cited**

OTHER PUBLICATIONS

Information and Technology (Cat. No. 94CH3571-5). IEEE. Part vol. 1, 1994, pp. 13-18 vol. 1. New York, NY, USA.
Krueerke, Daniel, "Speed May Give Ferroelectric LCOS Edge in Projection Race," Display Devices Fall '05. Copyright 2005 Dempa Publications, Inc. pp. 29-31.
Kuiper et al., "Variable-Focus Liquid Lens for Miniature Cameras," Applied Physics Letters 85:1128-1130 (2004).
Kuribayashi, et al., "A Method for Reproducing Apparent Continuous Depth in a Stereoscopic Display Using "Depth-Fused 3D" Technology" Journal of the Society for Information Display 14:493-498 (2006).
L. Brown and H. Hua, "Magic lenses for augmented virtual environments," IEEE Comput. Graphics Appl. 26, 64-73 (2006).
L. Davis, J. P. Rolland, F. Hamza-Lup, Y. Ha, J. Norfleet, and C. Imielinska, 'Enabling a continuum of virtual environment experiences,' IEEE Comput. Graphics Appl. 23, pp. 10-12 Mar./Apr. 2003.
L. G. Brown's: 'Applications of the Sensics panoramic HMD' SID Symposium Digest vol. 39, 2008, p. 77.
Laurence R. Young, David Sheena, "Survey of eye movement recording methods", Behavior Research Methods & Instrumentation, 7(5), 397-429, 1975.
Liu et al., 'A Novel Prototype for an Optical See-Through Head-Mounted Display with Addressable Focus Cues,' IEEE Transactions on Visualization and Computer Graphics 16:381-393 (2010).
Liu et al., "A Systematic Method for Designing Depth-Fused Multi-Focal Plane Three-Dimensional Displays," Optics Express 18:11562-11573 (2010).
Liu et al., "An Optical See-Through head Mounted Display with Addressable Focal Planes," IEEE Computer Society, pp. 33-42 (2008).
Liu et al., "Time-Multiplexed Dual-Focal Plane Head-Mounted Display with a Liquid Lens," Optics Letters 34:1642-1644 (2009).
Loschky, L.C. and Wolverton, G.S., "How late can you update gaze-contingent multiresolutional displays without detection?" ACM Trans. Mult. Comp. Comm. and App. 3, Nov. 2007.
Love et al. (High Speed switchable lens enables the development of a volumetric stereoscopic display. Aug. 2009, Optics Express. vol. 17, No. 18, pp. 15716-15725.).
M. Marti?nez-Corral, H. Navarro, R. Martinez-Cuenca, G. Saavedra, and B. Javidi, "Full parallax 3-D TV with programmable display parameters," Opt. Phot. News 22, 50-50 (2011).
M. D. Missig and G. M. Morris, "Diffractive optics applied to eyepiece design," Appl. Opt. 34, 2452-2461 (1995).
M. Daneshpanah, B. Javidi, and E. Watson, "Three dimensional integral imaging with randomly distributed sensors," Journal of Optics Express, vol. 16, Issue 9, pp. 6368-6377, Apr. 21, 2008.
M. Gutin: 'Automated design and fabrication of ocular optics' Proc. SPIE 2008, p. 7060.
M. Inami, N. Kawakami, and S. Tachi, 'Optical camouflage using retro-reflective projection technology,' in Proceedings of ISMAR 2003 {ISMAR, 2003).
M. Inami, N. Kawakami, D. Sekiguchi, Y. Yanagida, T. Maeda, and S. Tachi, "Visuo-haptic display using head-mounted projector," in Proceedings of IEEE Virtual Reality 2000, pp. 233-240.
Armitage, David, Ian Underwood, and Shin-Tson Wu. Introduction to Microdisplays. Chichester, England: Wiley, 2006.
Hoshi, et al, "Off-axial HMD optical system consisting of aspherical surfaces without rotational symmetry," Proc. SPIE 2653, Stereoscopic Displays and Virtual Reality Systems III, 234 (Apr. 10, 1996).
European Search Report dated Apr. 28, 2016 from EP application 13847218.8.
Xinda Hu et al: "48.1: Distinguished Student Paper: A Depth-Fused Multi-Focal-Plane Display Prototype Enabling Focus Cues in StereoscopicDisplays", SID International Symposium. Digest of Technical Papers, vol. 42, No. I, Jun. 1, 2011 (Jun. 1, 2011), pp. 691-694, XP055266326.
Y. Ha, H. Hua, R. Martins, and J. R Rolland, "Design of a wearable wide-angle projection color display," in Proceedings of International Optical Design Conference 2002 (IODC, 2002), pp. 67-73.
Yamazaki et al, "Thin wide-field-of-view HMD with free-form-surface prism and applications", Proc. SPIE 3639, Stereoscopic Displays and Virtual Reality Systems VI, 453 (May 24, 1999).
Yano, S., Emoto, M., Mitsuhashi, T., and Thwaites, H., "A study of visual fatigue and visual comfort for 3D HDTV/ HDTV images," Displays, 23(4), pp. 191-201, 2002.
Zhang, R., "8.3: Design of a Compact Light Engine for FLCOS Microdisplays in a p-HMPD system", Society for Information Display 2008 International Symposium, Seminar and Exhibition (SID2008), Los Angeles, CA, May 2008.
Zhang, R., et al., "Design of a Polarized Head-Mounted Projection Display Using Ferroelectric Liquid-Crystal-on-Silicon Microdisplays", Applied Optics, vol. 47, No. 15, May 20, 2008, pp. 2888-2896.
Zhang, R., et al., "Design of a Polarized Head-Mounted Projection Display using FLCOS Microdisplays", Proc. of SPIE vol. 6489, 64890B-1. (2007).
Hu and Hua, "Design and tolerance of a freeform optical system for an optical see-through multi-focal plane display," Applied Optics, 2015.
A. Yabe, "Representation of freeform surface suitable for optimization," Applied Optics, 2012.
M. L. Thomas, W. P. Siegmund, S. E. Antos, and R. M. Robinson, "Fiber optic development for use on the fiber optic helmet-mounted display", Helmet-Mounted Displays, J. T. Carollo, ed., Proc. SPIE 116, 90-101, 1989.
M. Lucente, "Interactive three-dimensional holographic displays: seeing the future in depth," Computer Graphics, 31(2), pp. 63-67, 1997.
M. Robinson. J. Chen, and G. Sharp, Polarization Engineering for LCD Projection. John Wiley & Sons, Ltd. England, 2005.
McQuaide et al., "A Retinal Scanning Display System That Produces Multiple Focal Planes with a Deformable Membrane Mirror," Displays 24:65-72 (2003).
Mon-Williams et al., "Binocular Vision in a Virtual World: Visual Deficits Following the Wearing of a Head-Mounted Display," Ophthalmic Physiol. Opt. 13:387-391 (1993).
N. Kawakami, M. Inami, D. Sekiguchi, Y. Yangagida, T. Maeda, and S. Tachi, 'Object-oriented displays: a new type of Display systemsfrom immersive display to object-oriented displays,' in Proceedings of IEEE SMC 1999, IEEE International Conference on Systems, Man, and Cybernetics, vol. 5, pp. 1066-1069.
O. Cakmakci, B. Moore, H. Foroosh, and J. P. Rolland, "Optimal local shape description for rotationally non-symmetric optical surface design and analysis," Opt. Express 16, 1583-1589 (2008).
Optical Research Associates, http://www.optica1res.com, 2 pages (obtained Jan. 26, 2011).
P. A. Blanche, et al, "Holographic three-dimensional telepresence using large-area photorefractive polymer", Nature, 168, 80-83, Nov. 2010.
P. Gabbur, H. Hua, and K. Barnard, 'A fast connected components labeling algorithm for real-time pupil detection,' Mach. Vision Appl., 21(5):779-787, 2010.
R. Azuma, A Survey of Augmented Reality in Presence; Teleoperators and Virtual Environments 6. 4, 355-385, (1997).
R. Kijima, K. Haza, Y. Tada, and T. Ojika, "Distributed display approach using PHMD with infrared camera," in Proceedings of IEEE 2002 Virtual Reality Annual International Symposium (IEEE, 2002), pp. 1-8.
R. Kijima and T. Ojika, "Transition between virtual environment and workstation environment with projective headmounted display," in Proceedings of IEEE VR 1997 (IEEE, 1997), pp. 130-137.
R. Martins, V. Shaoulov, Y. Ha, and J. P. Rolland, "Projection based head-mounted displays for wearable computers," Proc. SPIE 5442, 104-110 (2004).
R. Martinez-Cuenca, H. Navarro, G. Saavedra, B. Javidi, and M. Martinez-Corral, "Enhanced viewing-angle integral imaging by multiple-axis telecentric relay system," Optics Express, vol. 15, Issue 24, pp. 16255-16260, Nov. 21, 2007.

(56) **References Cited**

OTHER PUBLICATIONS

R. N. Berry, L. A. Riggs, and C. P. Duncan, "The relation of vernier and depth discriminations to field brightness," J. Exp. Psychol. 40, 349-354 (1950).
R. Schulein, C. Do, and B. Javidi, "Distortion-tolerant 3D recognition of underwater objects using neural networks," Journal of Optical Society of America A, vol. 27, No. 3, pp. 461-468, Mar. 2010.
R. Schulein, M. DaneshPanah, and B. Javidi, "3D imaging with axially distributed sensing," Journal of Optics Letters, vol. 34, Issue 13, pp. 2012-2014, Jul. 1, 2009.
R.J. Jacob, "The use of eye movements in human-computer interaction techniques: what you look at is what you get", ACM Transactions on Information Systems, 9(2), 152-69, 1991.
Reingold, E.M., L.C. Loschky, G.W. McConkie and D.M. Stampe, "Gaze-contingent multiresolutional displays: An integrative review," Hum. Factors 45, 307-328 (2003).
Rolland, J. P., A. Yoshida, L. D. Davis and J. H. Reif, "High-resolution inset head-mounted display," Appl. Opt. 37, 4183-93 (1998).
Rolland, J.P., et al., 'Optical versus video see-through head mounted displays in medical visualization', Presence' Teleoperators and Virtual Environments 9, 287-309 (2000).
Rolland et al., "Multifocal Planes Head-Mounted Displays," Applied Optics 39:3209-3215 (2000).
S. Bagheri and B. Javidi, "Extension of Depth of Field Using Amplitude and Phase Modulation of the Pupil Function," Journal of Optics Letters, vol. 33, No. 7, pp. 757-759, Apr. 1, 2008.
S. Hong, J. Jang, and B. Javidi,"Three-dimensional volumetric object reconstruction using computational integral imaging," Journal of Optics Express, on-line Journal of the Optical Society of America, vol. 12, No. 3, pp. 483-491, Feb. 9, 2004.
S. Hong and B. Javidi, "Distortion-tolerant 3D recognition of occluded objects using computational integral imaging," Journal of Optics Express, vol. 14, Issue 25, pp. 12085-12095, Dec. 11, 2006.
S. Kishk and B. Javidi, "Improved Resolution 3D Object Sensing and Recognition using time multiplexed Computational Integral Imaging," Optics Express, on-line Journal of the Optical Society of America, vol. 11, No. 26, pp. 3528-3541, Dec. 29, 2003.
Schowengerdt, B. T., and Seibel, E. J., "True 3-D scanned voxel displays using single or multiple light sources," Journal of SID, 14(2), pp. 135-143, 2006.
Schowengerdt et al., "True 3-D Scanned Voxel Displays Using Single or Multiple Light Sources," J. Soc. Info. Display 14:135-143 (2006).
Sheedy et al., "Performance and Comfort on Near-Eye Computer Displays," Optometry and Vision Science 79:306-312 (2002).
Shibata et al., "Stereoscopic 3-D Display with Optical Correction for the Reduction of the Discrepancy Between Accommodation and Convergence," Journal of the Society for Information Display 13:665-671 (2005).
Shiwa et al., "Proposal for a 3-D Display with Accommodative Compensation: 3DDAC," Journal of the Society for Information Display 4:255-261 (1996).
Sullivan, "A Solid-State Multi-Planar Volumetric Display," SID Symposium Digest of Technical Papers 34:354-356 (2003).
Suyama, S., Ohtsuka, S., Takada, H., Uehira, K., and Sakai, S., "Apparent 3D image perceived from luminance-modulated two 2D images displayed at different depths," Vision Research, 44: 785-793, 2004.
T. Okoshi, "Optimum design and depth resolution of lens-sheet and projection-type three-dimensional displays," Appl. Opt. 10, 2284-2291 (1971).
T. Ando, K. Yamasaki, M. Okamoto, and E. Shimizu, "Head Mounted Display using holographic optical element," Proc. SPIE, vol. 3293, 183 (1998).
Tibor Balogh, "The HoloVizio System," Proceedings of SPIE, VOI 6055, 2006.
Varioptic, "Video Auto Focus and Optical Image Stabilization," http://www.varioptic.com/en/home.html, 2 pages (2008).
Wann et al., Natural Problems for Stereoscopic Depth Perception in Virtual Environments, Vision Res. 35:2731-2736 (1995).
Wartenberg, Philipp, "EyeCatcher, the Bi-directional OLED Microdisplay," Proc. of SID 2011.
Watt et al., "Focus Cues Affect Perceived Depth," J Vision 5:834-862 (2005).
Winterbottom, M., et al., 'Helmet-Mounted Displays for use in Air Force Training and Simulation', Human Effectiveness Directorate, Nov. 2005, pp. 1-54.
Written Opinion dated Feb. 10, 2011 from PCT/CN2010/072376.
Written Opinion dated Jun. 18, 2010 in corresponding international application PCT/US2010/031799.
Written Opinion of the International Searching Authority dated Mar. 9, 2009 with regard to International Patent Application No. PCT/US2009/031606.
X. Hu and H. Hua, "Design and assessment of a depth-fused multi-focal-plane display prototype," Journal of Display Technology, Dec. 2013.
Xiao Xiao, Bahram Javidi, Manuel Martinez-Corral, and Adrian Stern , "Advances in Three-Dimensional Integral Imaging: Sensing, Display, and Applications," Applied Optics, 52(4):. 546-560,2013.
Xin Shen, Yu-Jen Wang, Hung-Shan Chen, Xiao Xiao, Yi-Hsin Lin, and Bahram Javidi, "Extended depth-of-focus 3D micro integral imaging display using a bifocal liquid crystal lens," Optics Letters, vol. 40, issue 4, pp. 538-541 (Feb. 9, 2015).
Xinda Hu and Hong Hua, "High-resolution optical see-through multi-focal-plane head-mounted display using freeform optics," Optics Express,22(11): 13896-13903, Jun. 2014.
Y. Takaki, Y. Urano, S. Kashiwada, H. Ando, and K. Nakamura, "Super multi-view winshield display for long-distance image information presentation," Opt. Express, 19, 704-16, 2011.
S. Feiner, 2002, "Augmented reality: A new way of seeing," Scientific American, No. 54, 2002.
K. Ukai and P.A. Howardth, "Visual fatigue caused by viewing stereoscopic motion images: background, theories, and observations," Displays, 29(2), pp. 106-116, 2008.
B. T. Schowengerdt, M. Murari, E. J. Seibel, "Volumetric display using scanned fiber array," SID Symposium Digest of Technical Papers, 2010.
H. Hua and B. Javidi, "A 3D integral imaging optical see-through head-mounted display", Optics Express, 22(11): 13484-13491, 2014.
W. Song, Y. Wang. D. Cheng, Y. Liu, "Light field head-mounted display with correct focus cue using micro structure array," Chinese Optics Letters, 12(6): 060010, 2014.
T. Peterka, R. Kooima, D. Sandin, A. Johnson, J. Leigh, T. DeFanti, "Advances in the Dynallax solid-state dynamic parallax barrier autostereoscopi visualization display system," IEEE Trans. Visua. Comp. Graphics, 14(3): 487-499, 2008.
Hu, X., Development of the Depth-Fused Multi-Focal Plane Display Technology, Ph.D. Dissertation, College of Optical Sciences, University of Arizona, 2014.
S. Ravikumar, K. Akeley, and M. S. Banks, "Creating effective focus cues in multi-plane 3D displays," Opt. Express 19, 20940-20952, 2011.
X. Hu and H. Hua, "Design and tolerance of a free-form optical system for an optical see-hrough multi-focal-plane display," Applied Optics, 54(33): 9990-9, 2015.
Dewen Cheng et al.; "Large field-of-view and high resolution free-form head-mounted display"; SPIE-OSA/ vol. 7652 Jun. 2018.

* cited by examiner

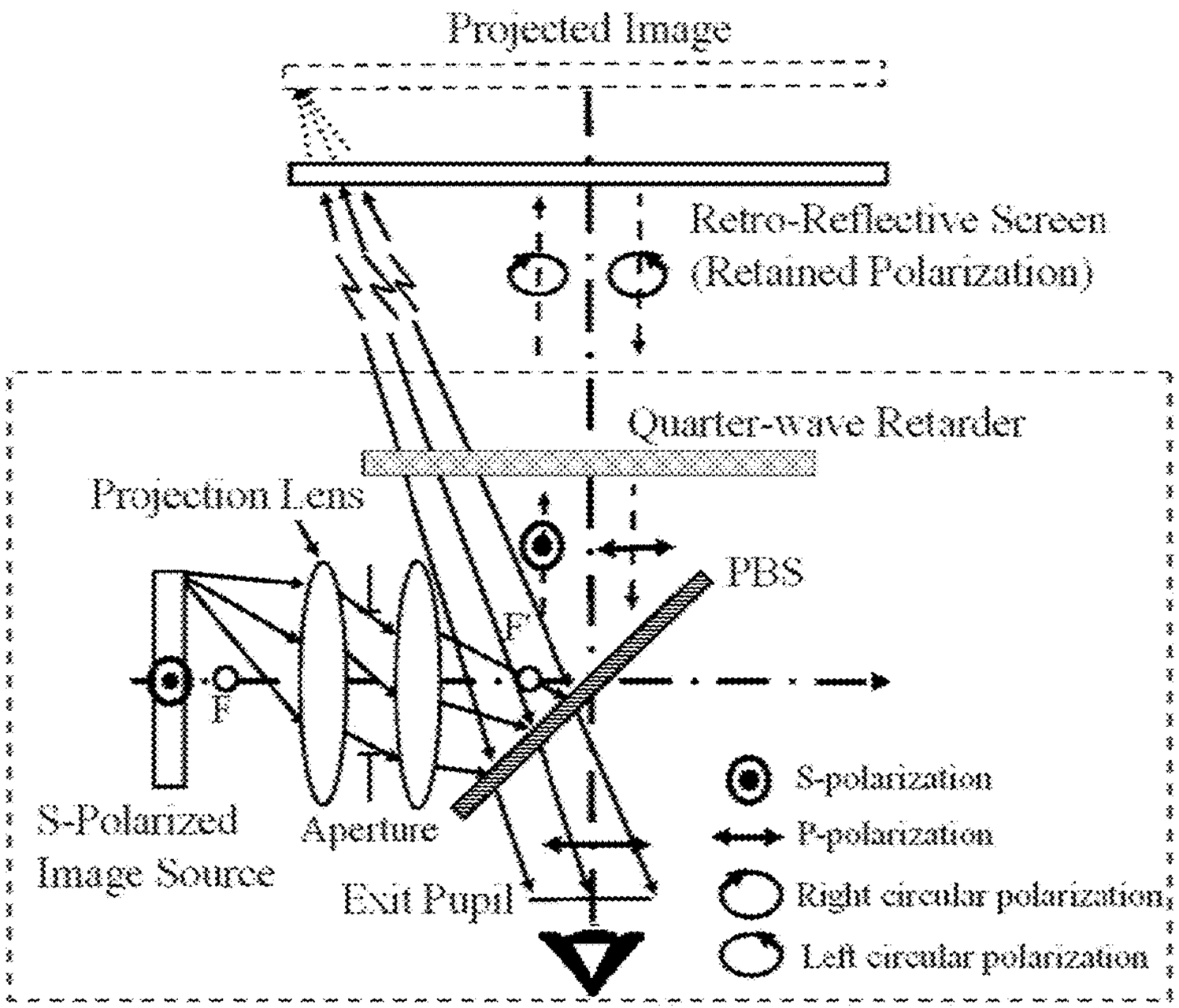
Projected Image
Retro-Reflective Screen
(Retained Polarization)
Quarter-wave Retarder
Projection Lens
PBS
S-Polarized
Image Source
Aperture
Exit Pupil
S-polarization
P-polarization
Right circular polarization
Left circular polarization

FIG. 1

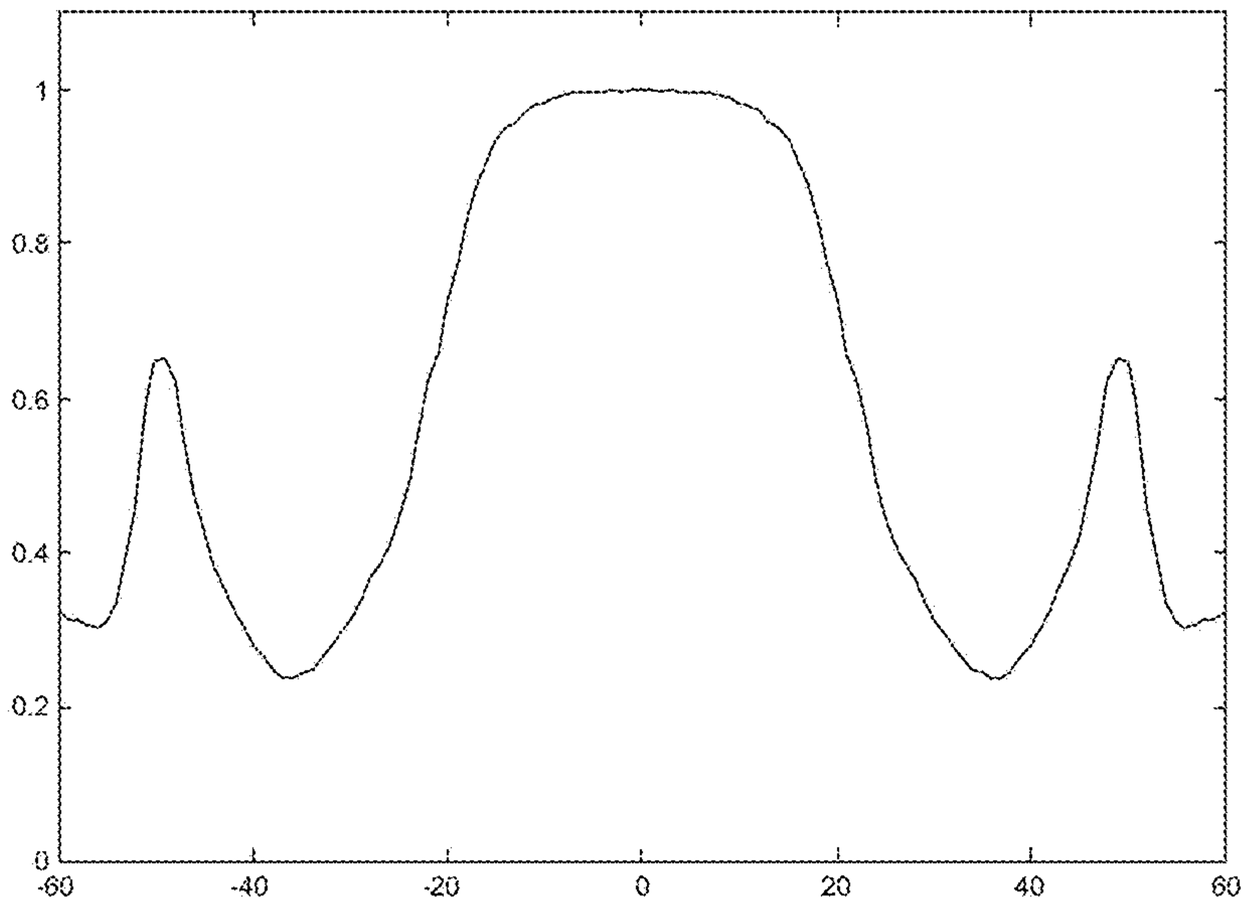
1
0.8
0.6
0.4
0.2
0
-60
-40
-20
0
20
40
60

FIG. 2

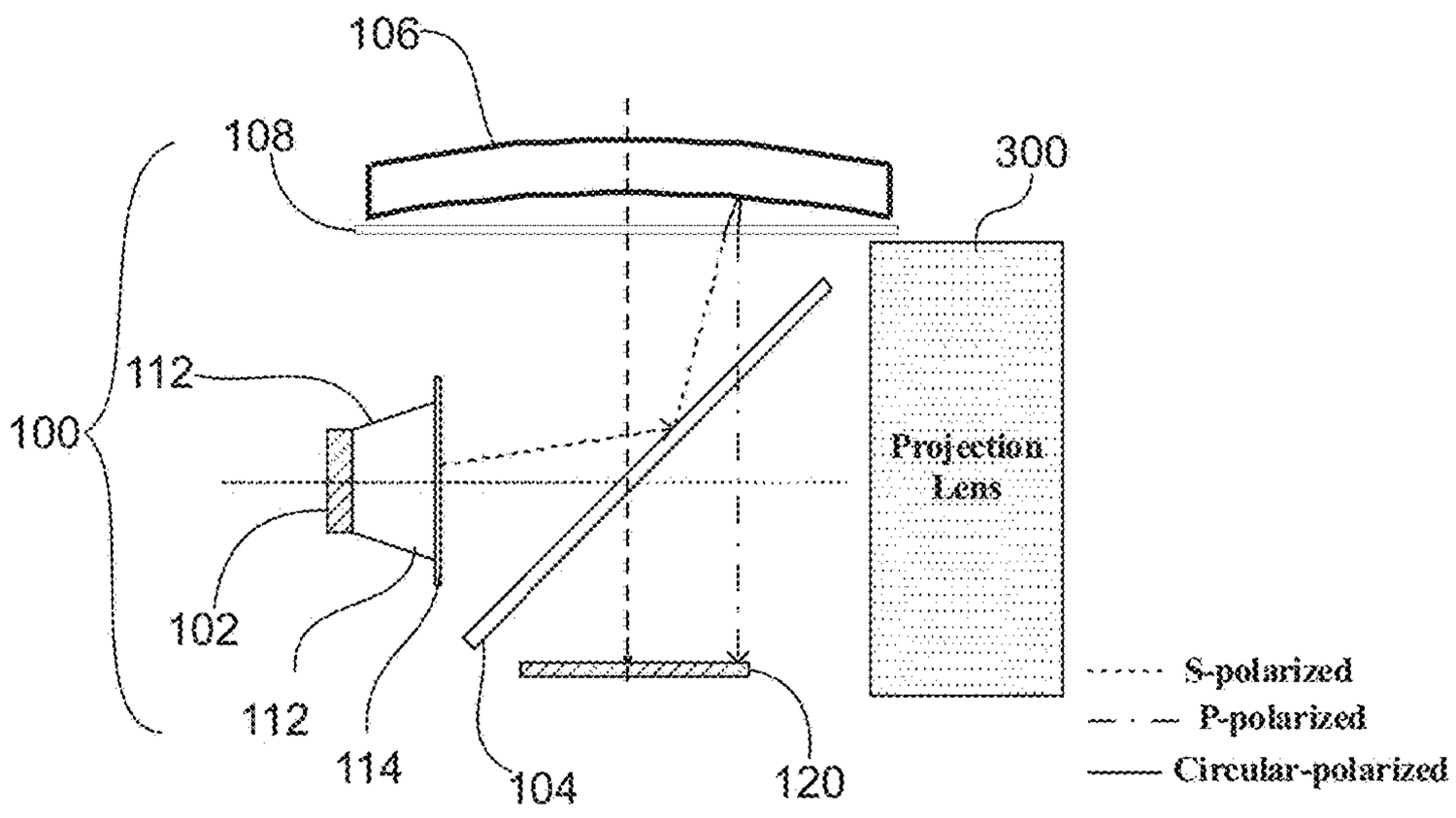
106
108
300
112
100
102
112
114
104
120
Projection Lens
S-polarized
P-polarized
Circular-polarized

FIG. 3

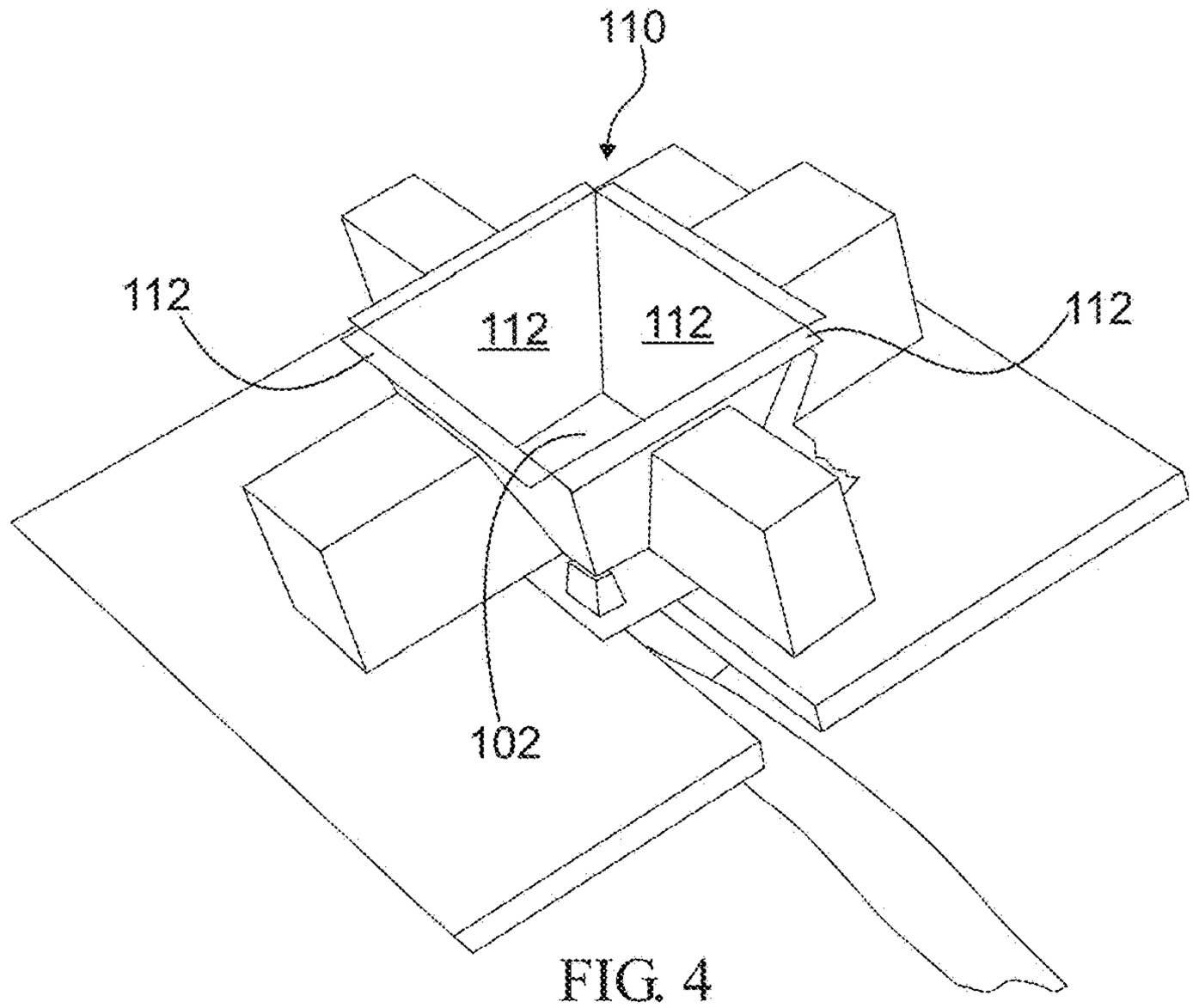

FIG. 4

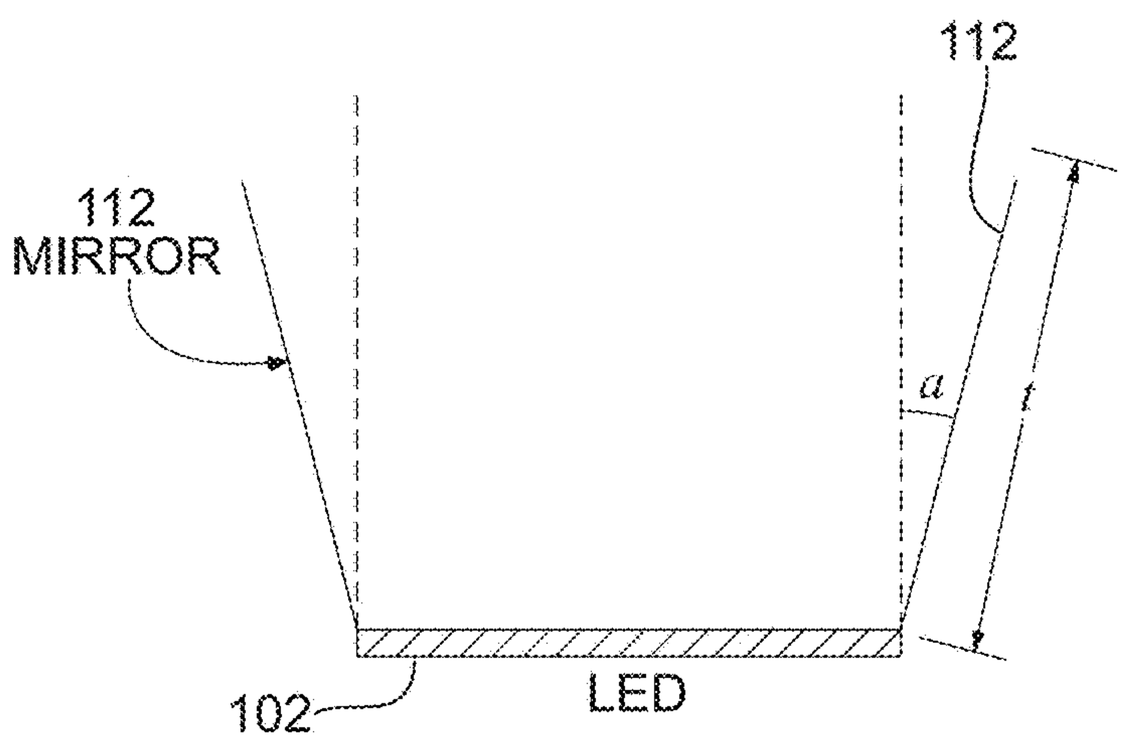

FIG. 5

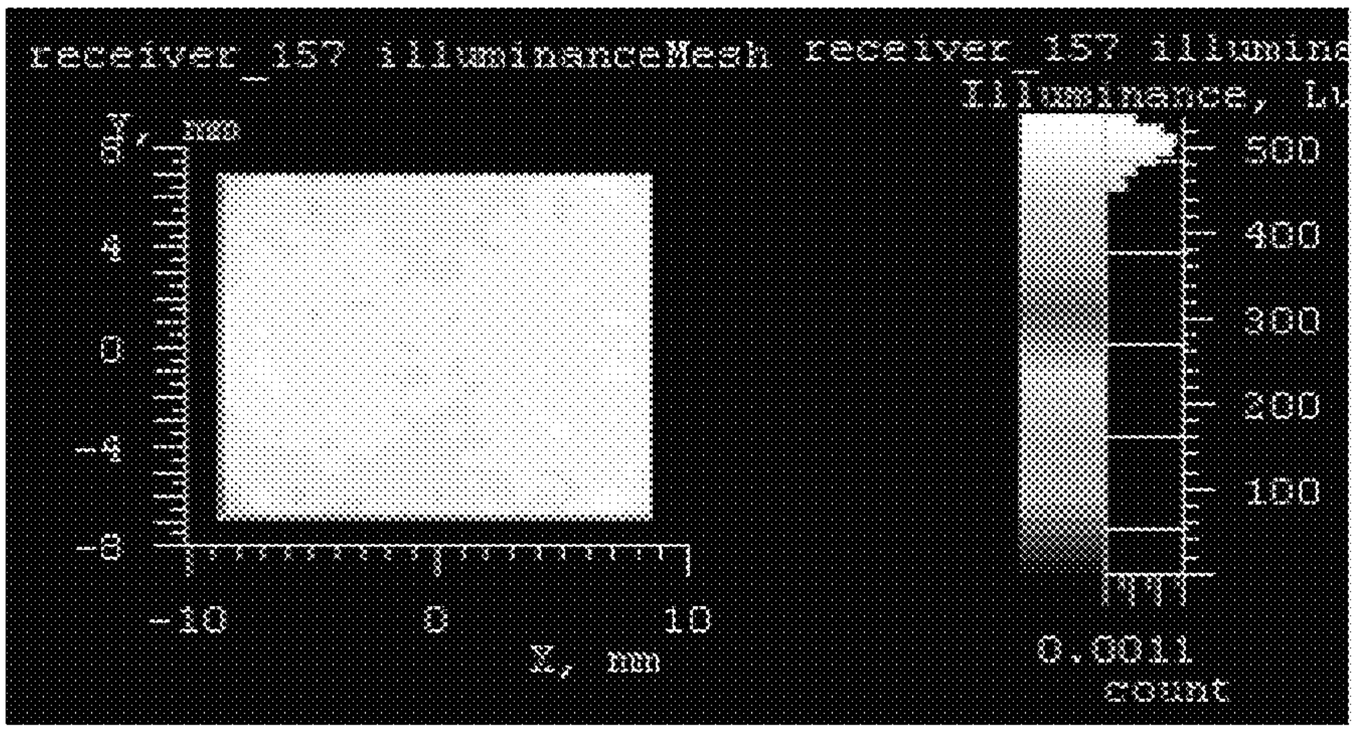
receiver_157 illuminanceMesh
Illuminance, Lux
Y, mm
8
4
0
-4
-8
-10
0
10
X, mm
500
400
300
200
100
0.0011
count

FIG. 6A

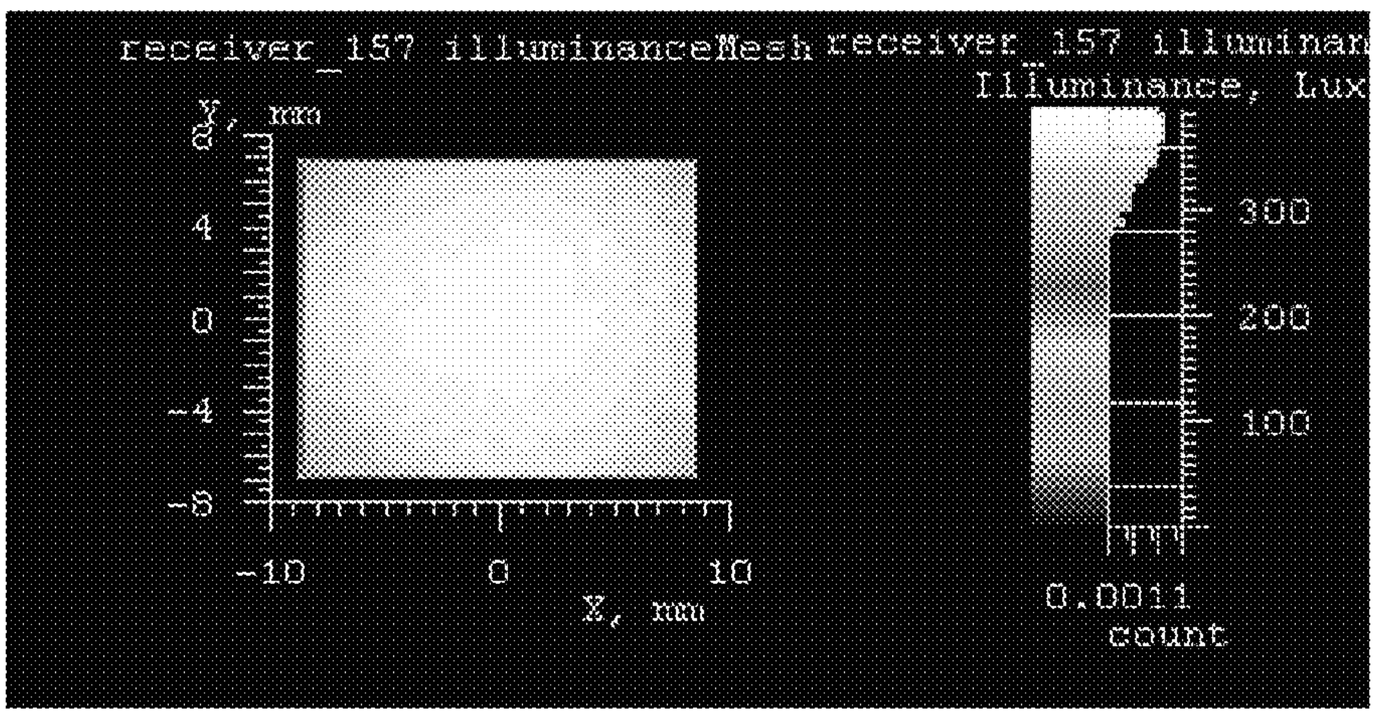
receiver_157 illuminanceMesh
Illuminance, Lux
Y, mm
8
4
0
-4
-8
-10
0
10
X, mm
300
200
100
0.0011
count

FIG. 6B

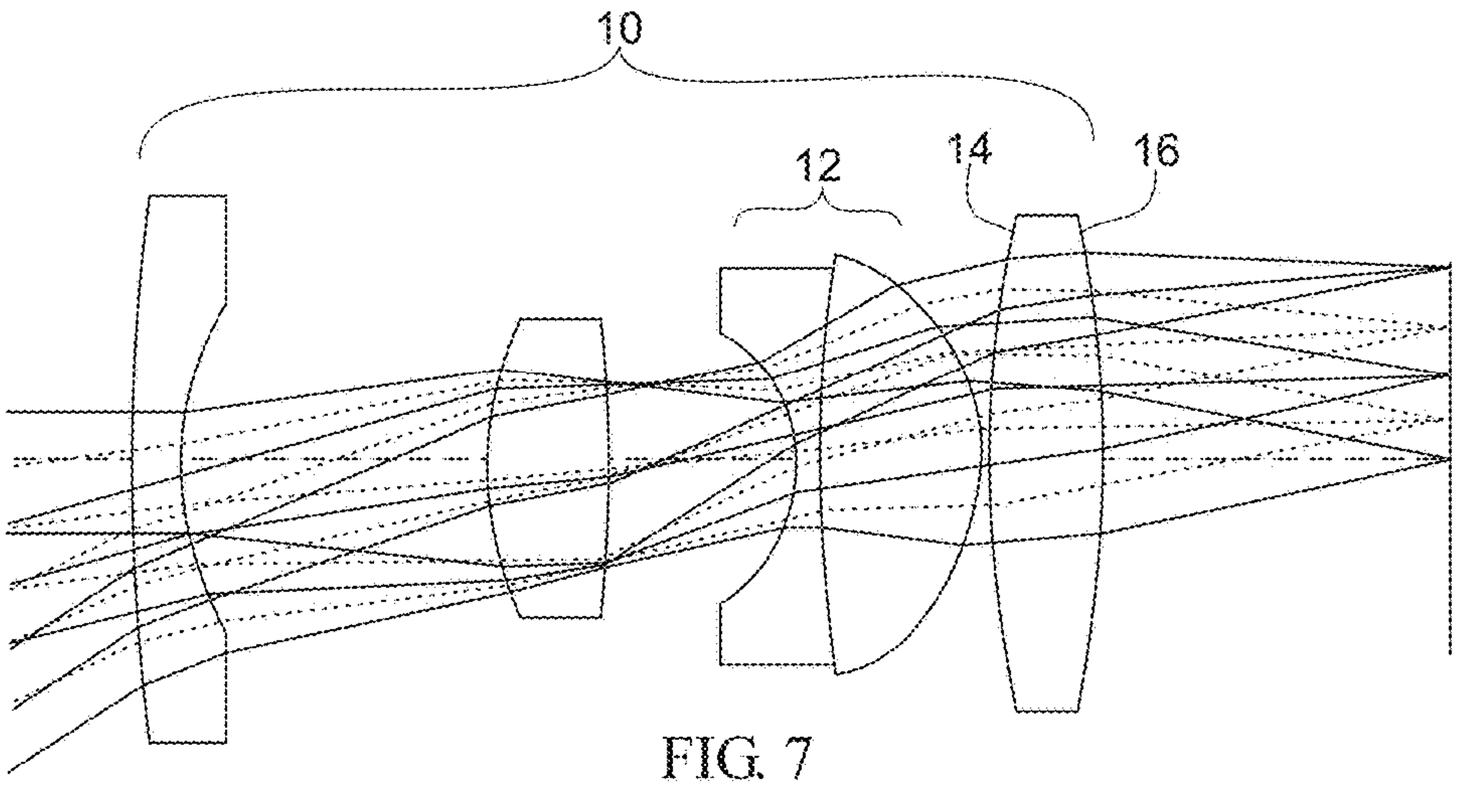

FIG. 7

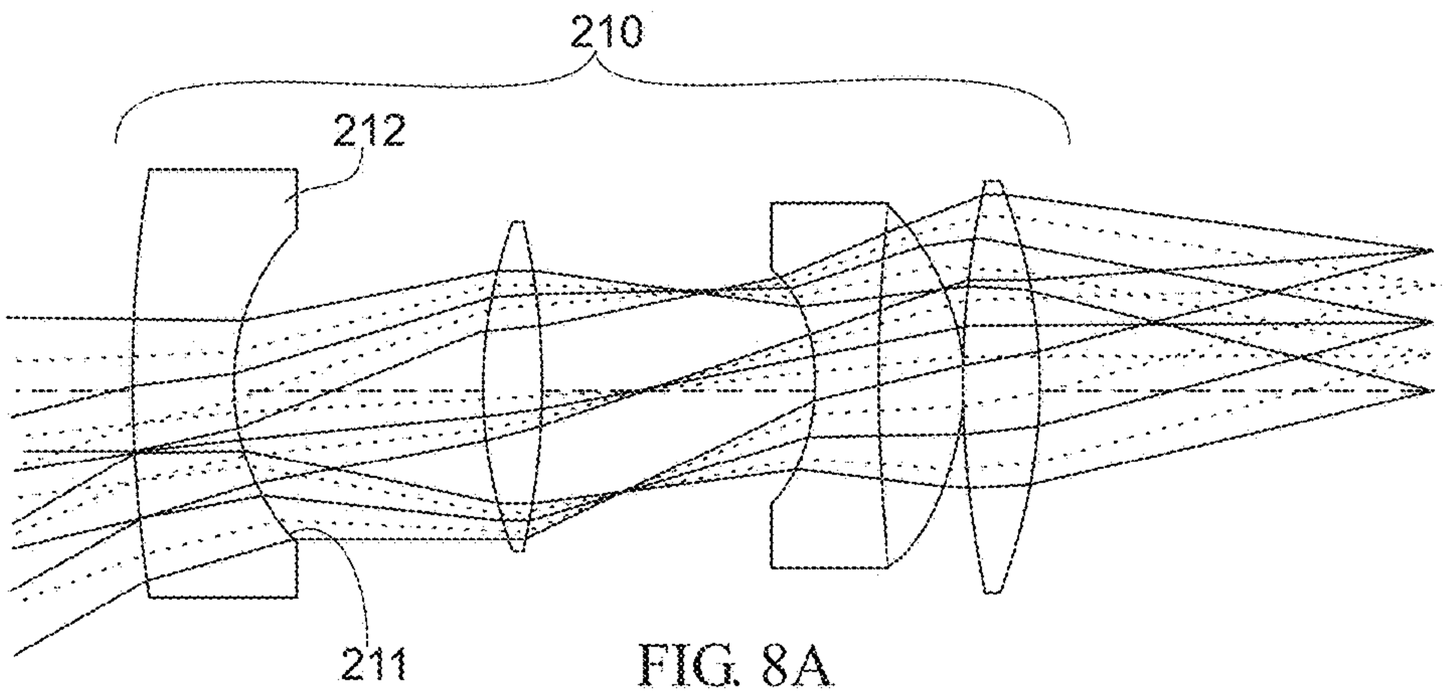

FIG. 8A

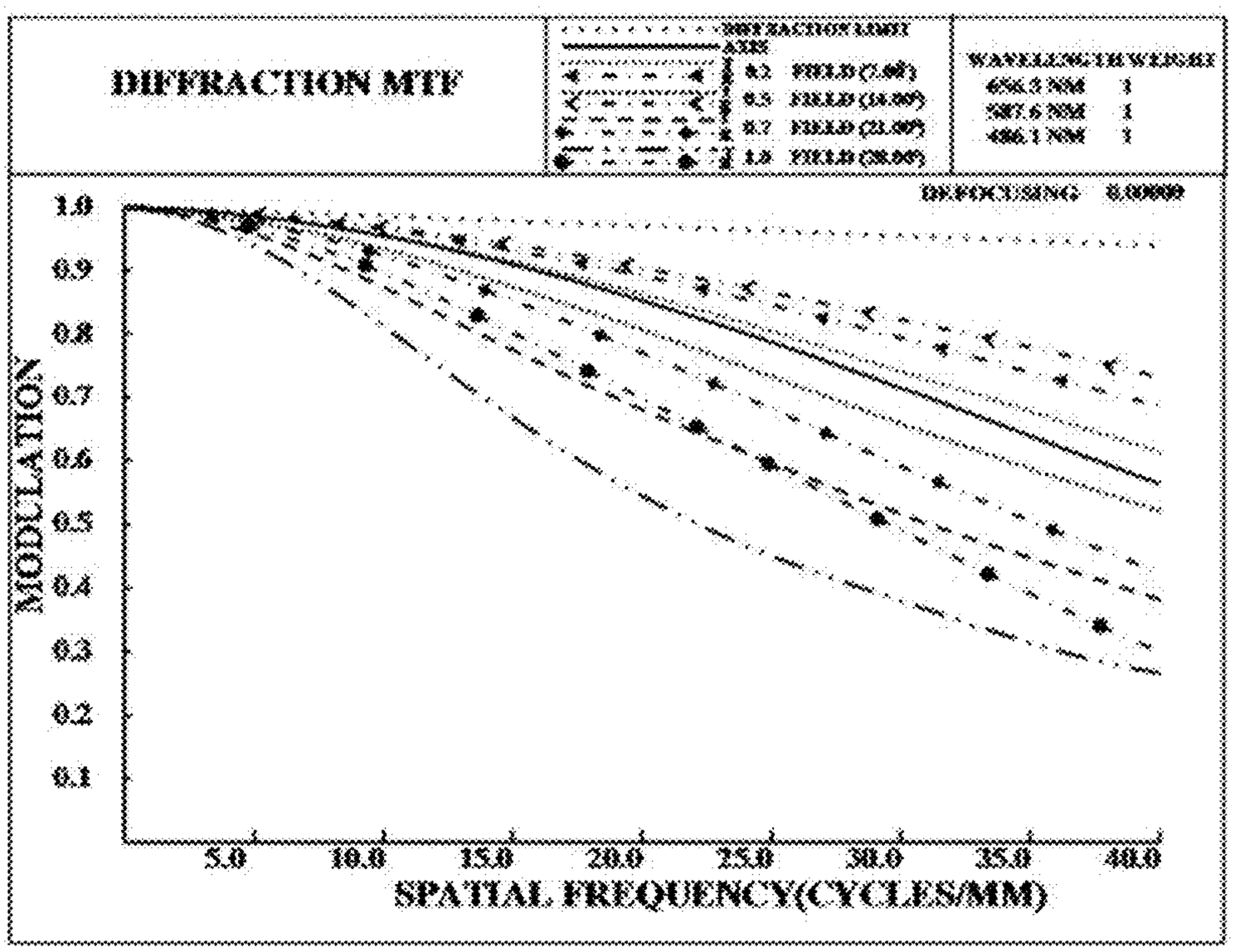
DIFFRACTION MTF
1.0
0.9
0.8
0.7
0.6
0.5
0.4
0.3
0.2
0.1
MODULATION
5.0
10.0
15.0
20.0
25.0
30.0
35.0
40.0
SPATIAL FREQUENCY(CYCLES/MM)

FIG. 8B

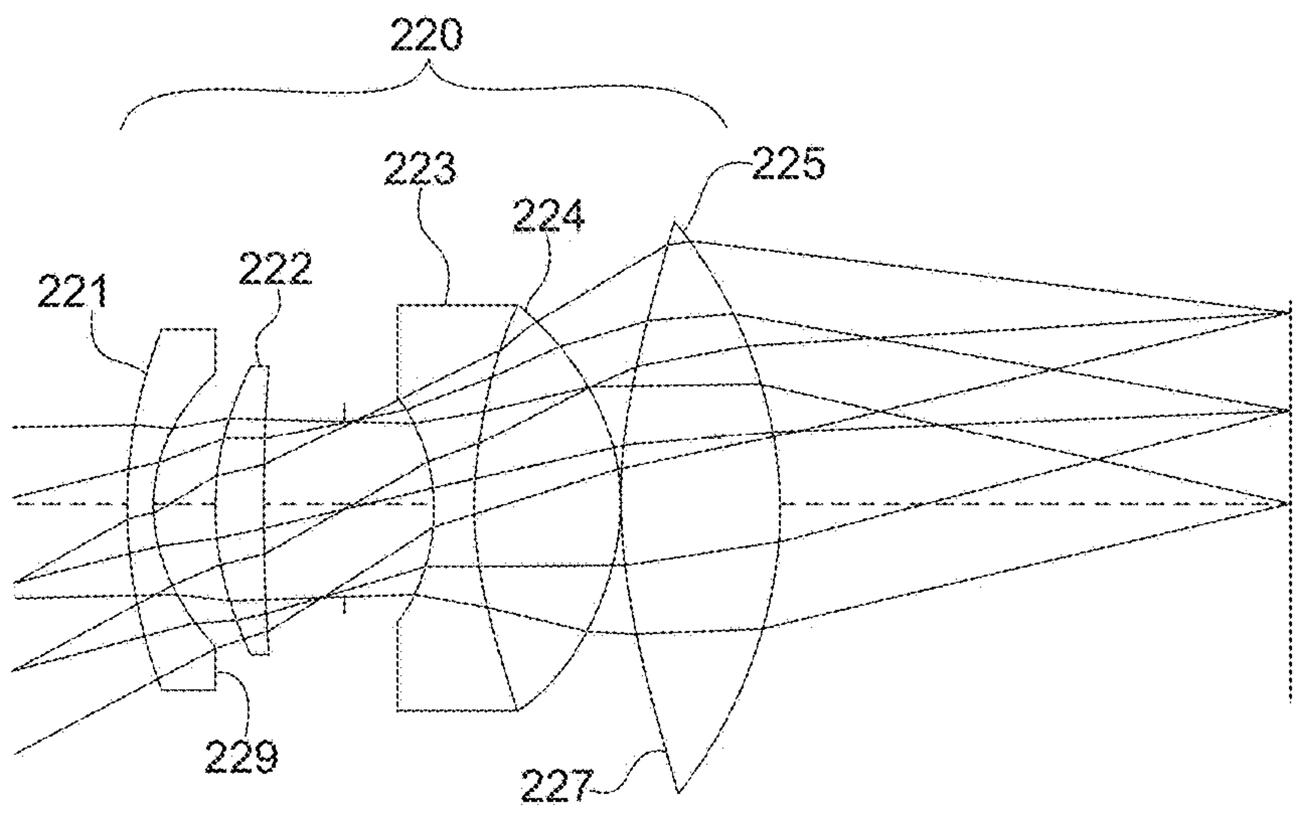
220
221
222
223
224
225
227
229

FIG. 9A

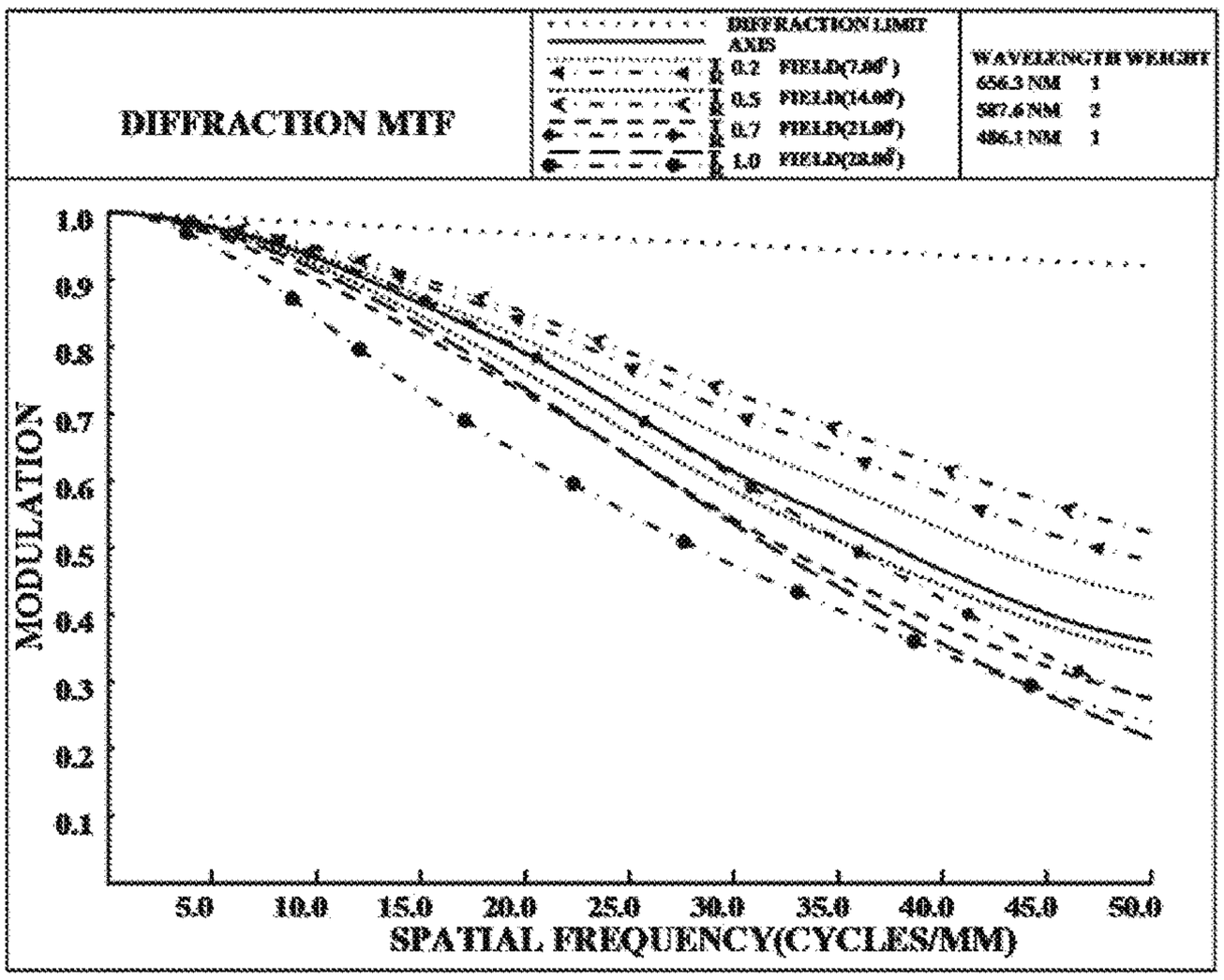
DIFFRACTION MTF
DIFFRACTION LIMIT
AXIS
0.2 FIELD(7.00°)
0.5 FIELD(14.00°)
0.7 FIELD(21.00°)
1.0 FIELD(28.00°)
WAVELENGTH WEIGHT
656.3 NM 1
587.6 NM 2
486.1 NM 1
MODULATION
1.0
0.9
0.8
0.7
0.6
0.5
0.4
0.3
0.2
0.1
5.0
10.0
15.0
20.0
25.0
30.0
35.0
40.0
45.0
50.0
SPATIAL FREQUENCY(CYCLES/MM)

FIG. 9B

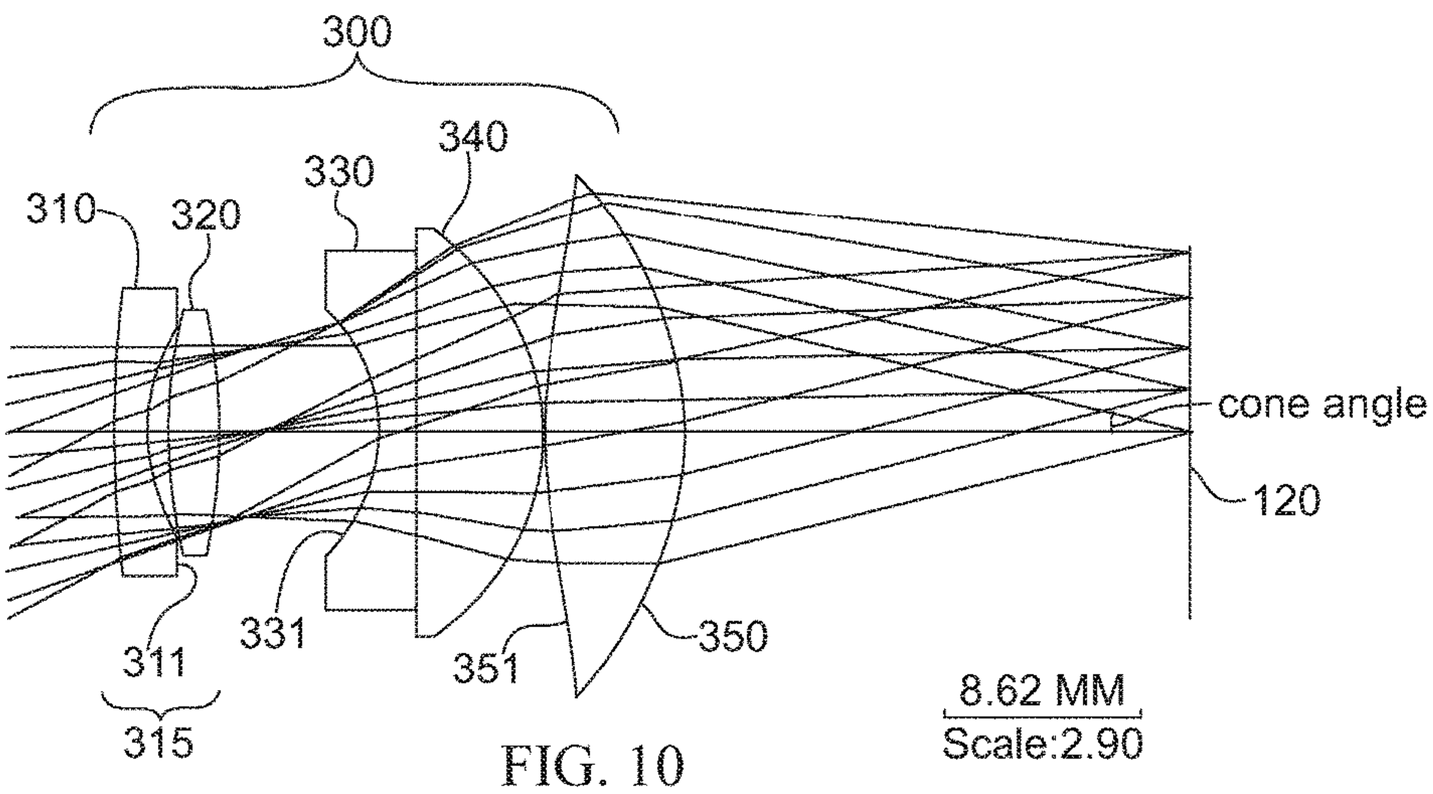
300
340
330
310
320
cone angle
120
331
311
351
350
315
8.62 MM
Scale:2.90

FIG. 10

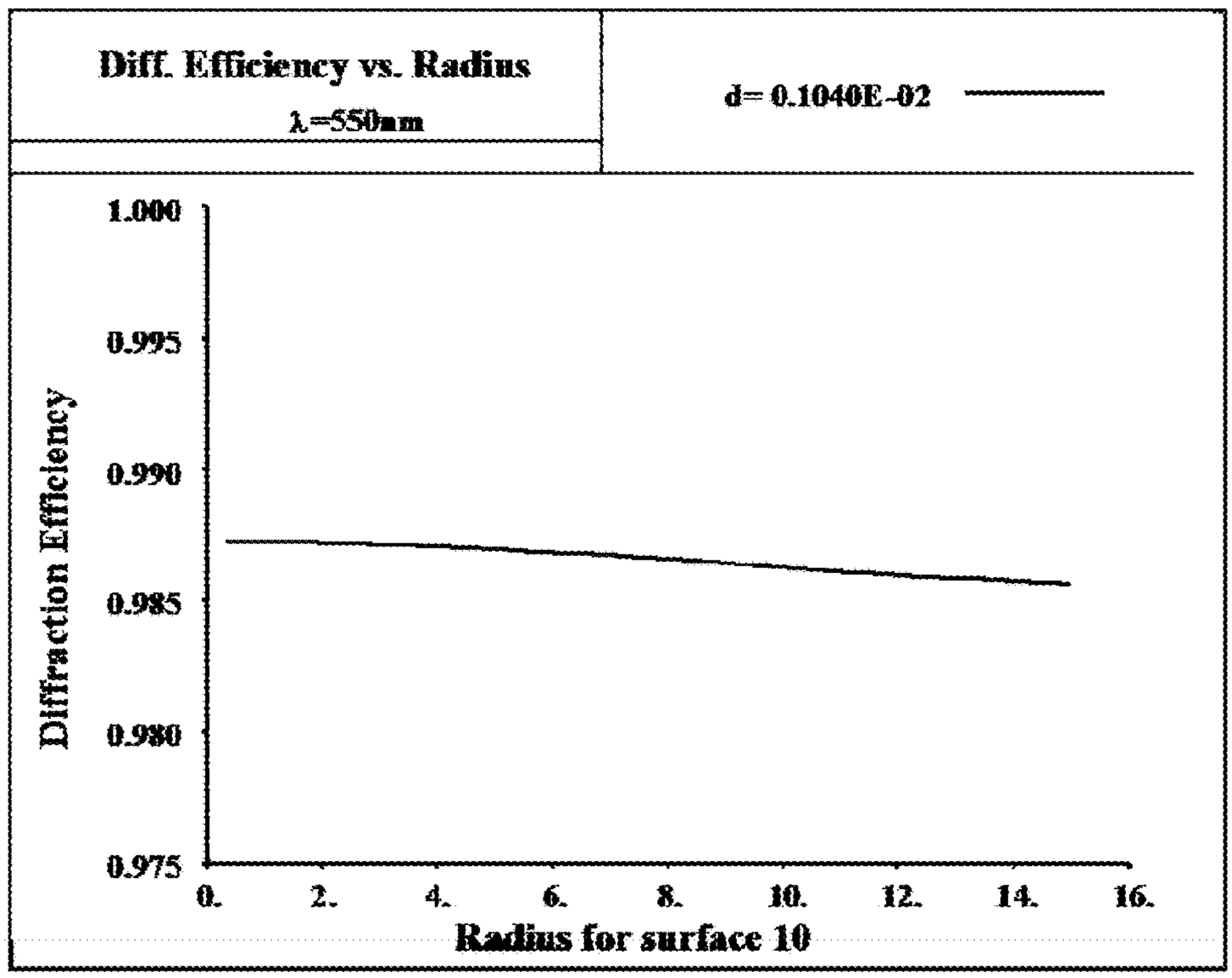
Diff. Efficiency vs. Radius
λ=550nm
d= 0.1040E-02
Diffraction Efficiency
1.000
0.995
0.990
0.985
0.980
0.975
0.
2.
4.
6.
8.
10.
12.
14.
16.
Radius for surface 10

FIG. 11A

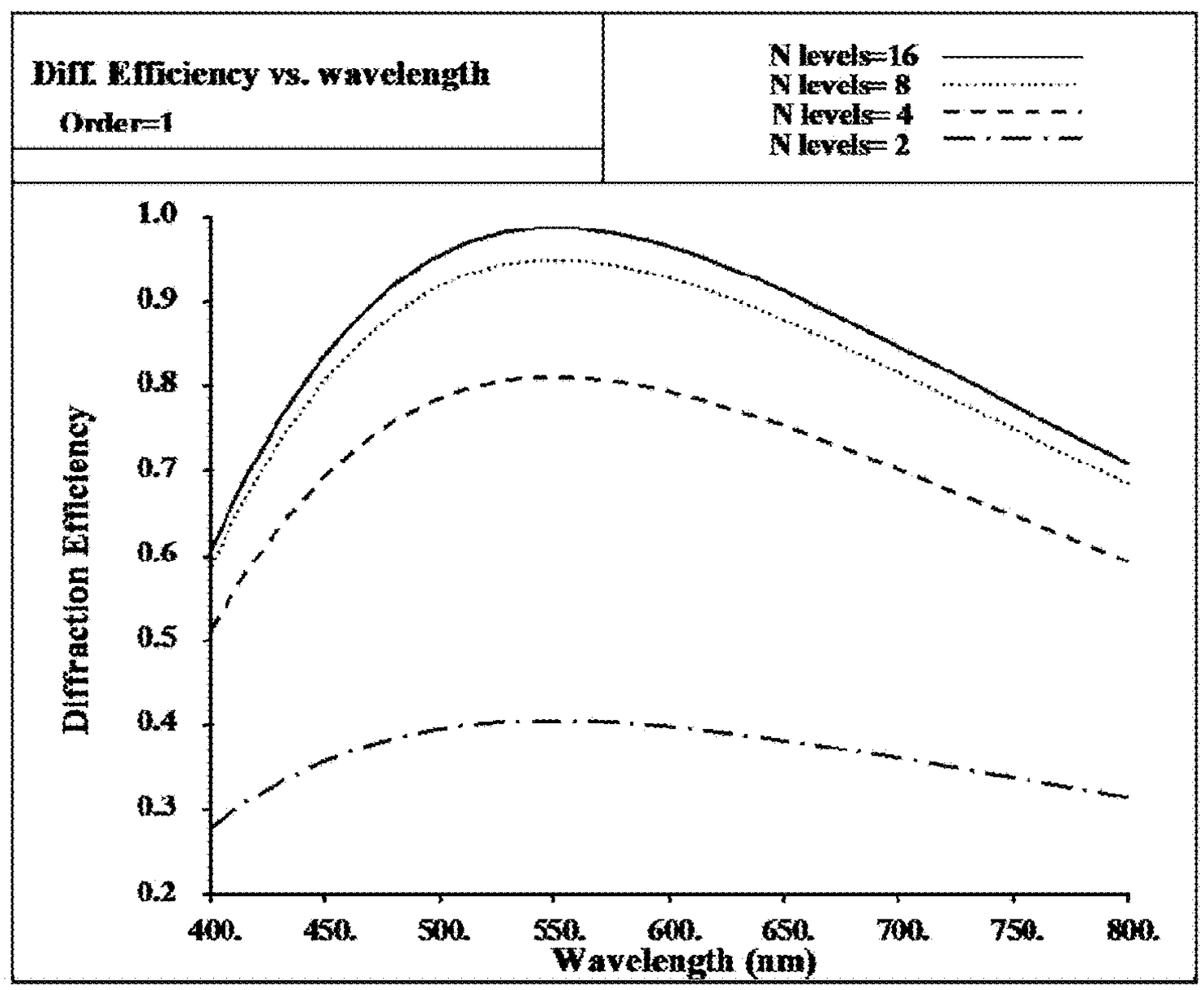
Diff. Efficiency vs. wavelength
Order=1
N levels=16
N levels= 8
N levels= 4
N levels= 2
Diffraction Efficiency
1.0
0.9
0.8
0.7
0.6
0.5
0.4
0.3
0.2
400.
450.
500.
550.
600.
650.
700.
750.
800.
Wavelength (nm)

FIG. 11B

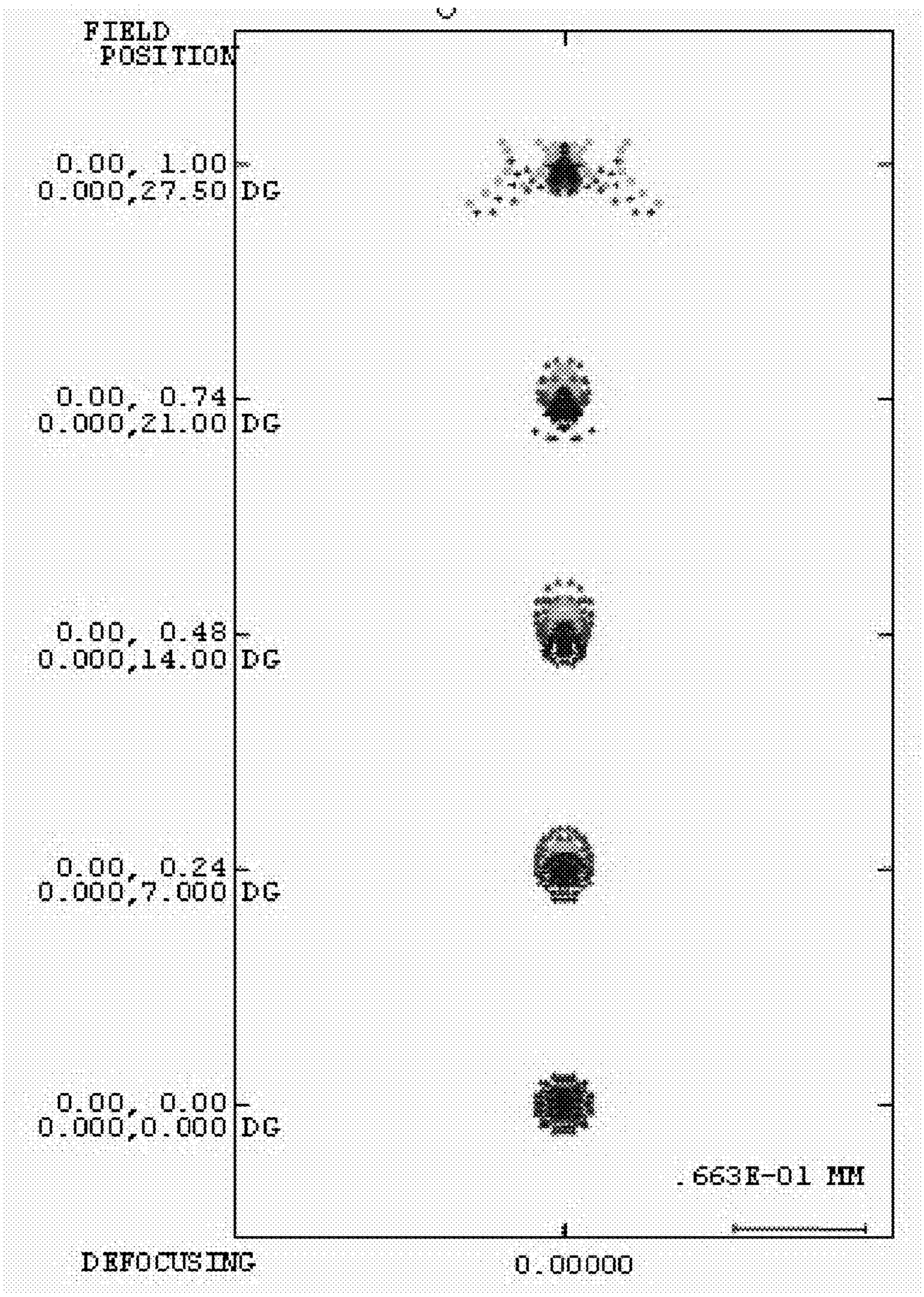
FIELD
POSITION
0.00, 1.00
0.000,27.50 DG
0.00, 0.74
0.000,21.00 DG
0.00, 0.48
0.000,14.00 DG
0.00, 0.24
0.000,7.000 DG
0.00, 0.00
0.000,0.000 DG
.663E-01 MM
DEFOCUSING
0.00000

FIG. 12A

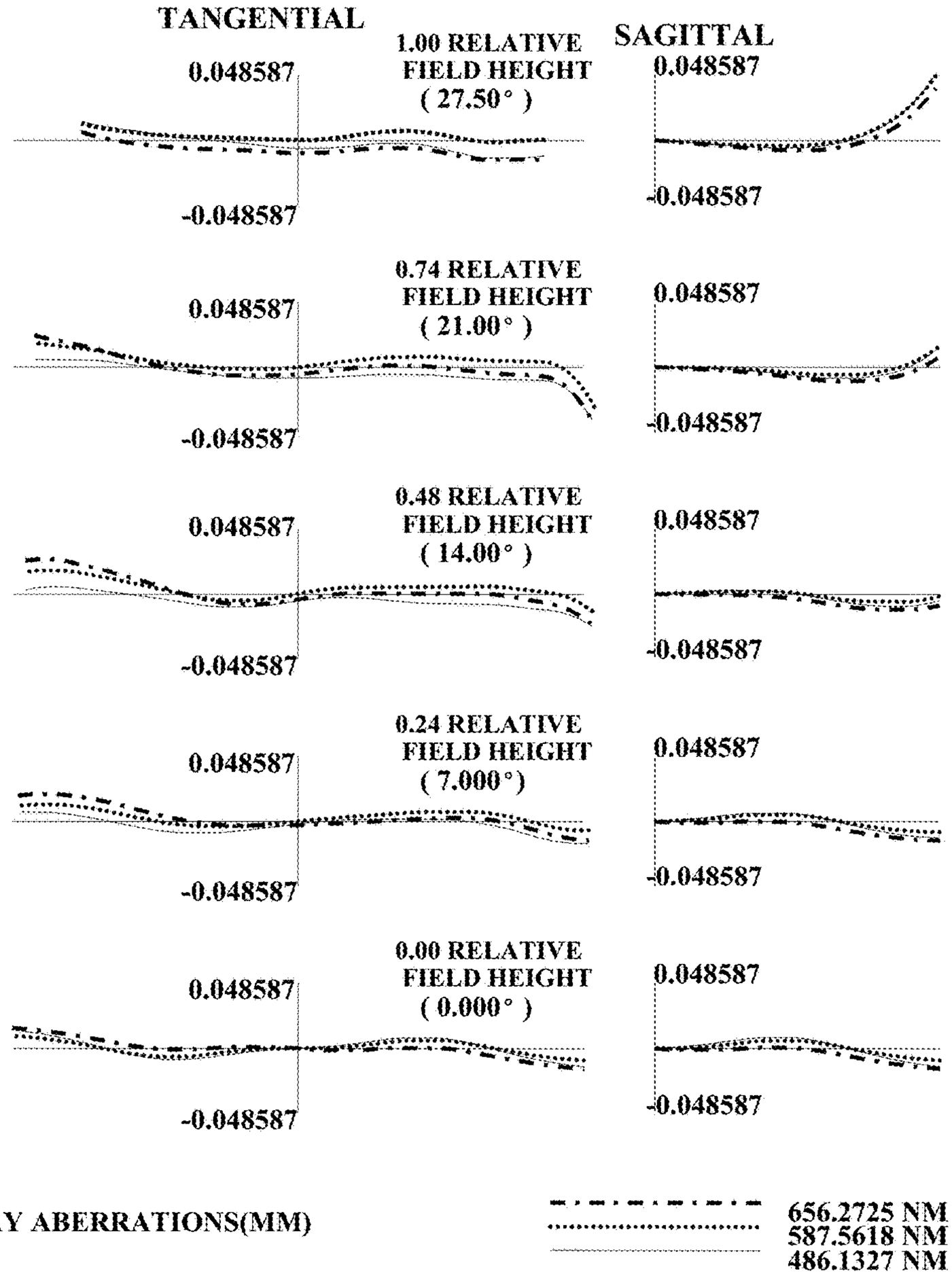
TANGENTIAL
SAGITTAL
1.00 RELATIVE FIELD HEIGHT (27.50°)
0.048587
-0.048587
0.74 RELATIVE FIELD HEIGHT (21.00°)
0.48 RELATIVE FIELD HEIGHT (14.00°)
0.24 RELATIVE FIELD HEIGHT (7.000°)
0.00 RELATIVE FIELD HEIGHT (0.000°)
RAY ABERRATIONS(MM)
656.2725 NM
587.5618 NM
486.1327 NM

FIG. 12B

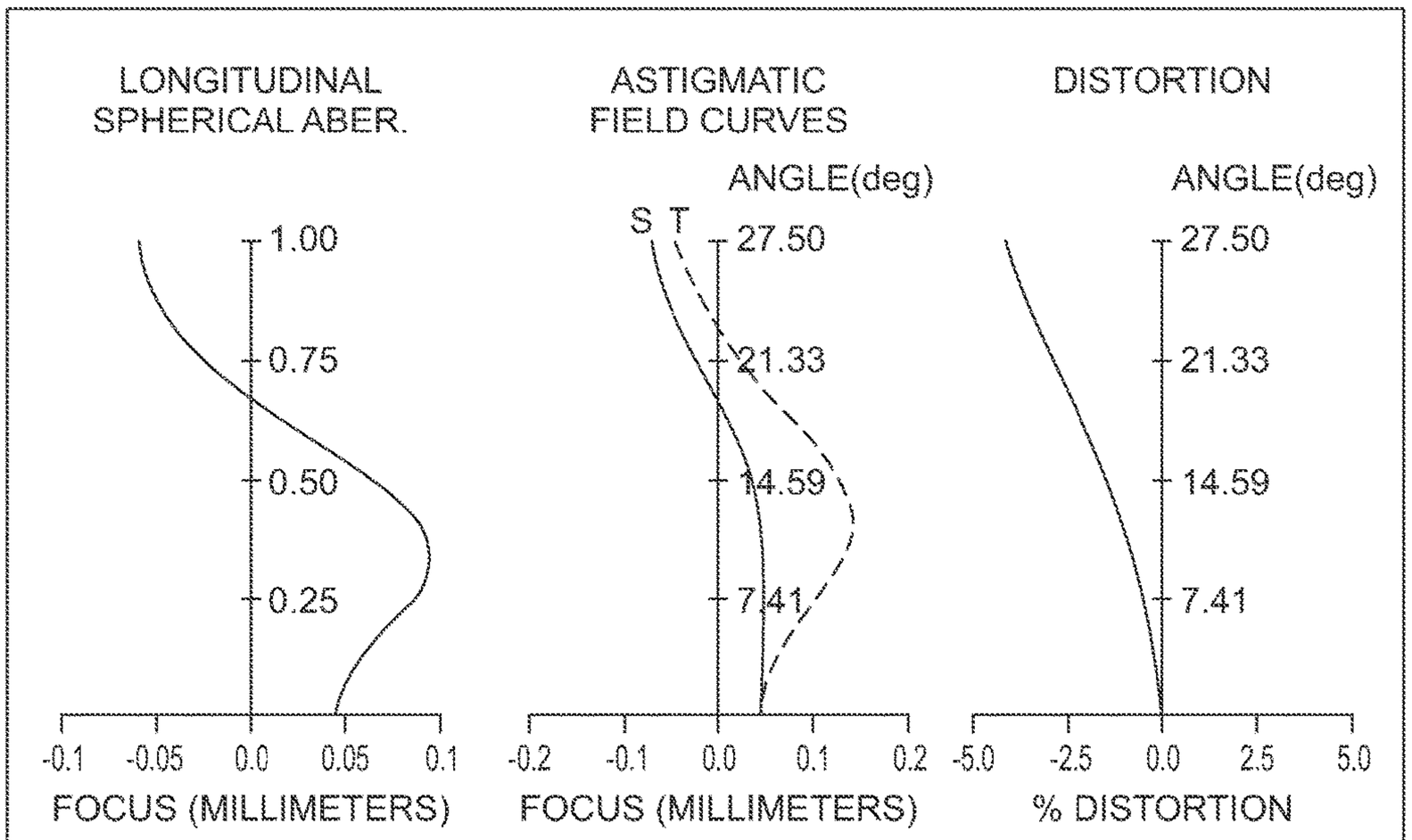
LONGITUDINAL
SPHERICAL ABER.
1.00
0.75
0.50
0.25
-0.1
-0.05
0.0
0.05
0.1
FOCUS (MILLIMETERS)
ASTIGMATIC
FIELD CURVES
ANGLE(deg)
S
T
27.50
21.33
14.59
7.41
-0.2
-0.1
0.0
0.1
0.2
FOCUS (MILLIMETERS)
DISTORTION
ANGLE(deg)
27.50
21.33
14.59
7.41
-5.0
-2.5
0.0
2.5
5.0
% DISTORTION
PROJECTION LENS_pHMPD_3DVIS_2008 (450nm)

FIG. 12C

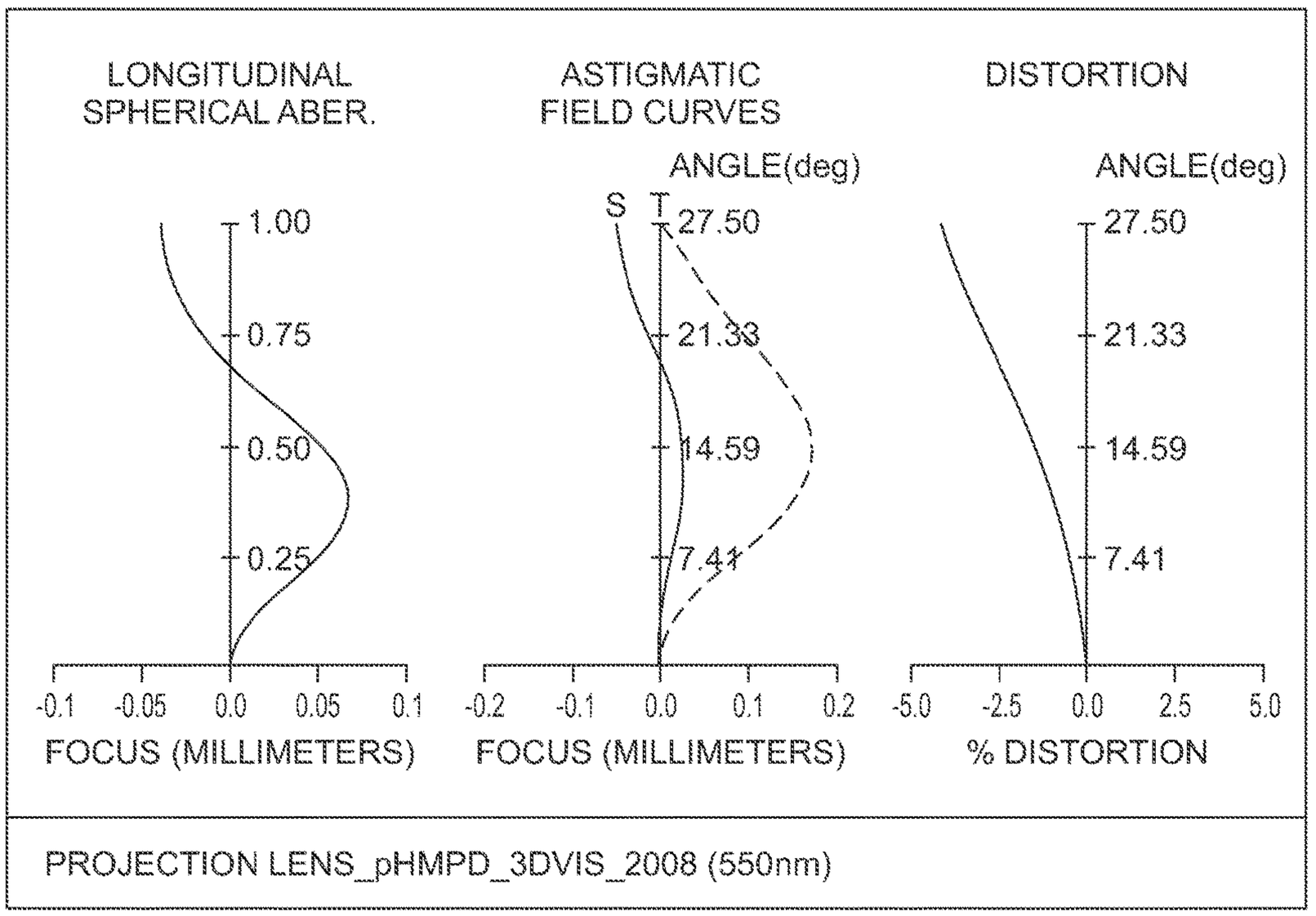
LONGITUDINAL
SPHERICAL ABER.
1.00
0.75
0.50
0.25
-0.1
-0.05
0.0
0.05
0.1
FOCUS (MILLIMETERS)
ASTIGMATIC
FIELD CURVES
ANGLE(deg)
S
T
27.50
21.33
14.59
7.41
-0.2
-0.1
0.0
0.1
0.2
FOCUS (MILLIMETERS)
DISTORTION
ANGLE(deg)
27.50
21.33
14.59
7.41
-5.0
-2.5
0.0
2.5
5.0
% DISTORTION
PROJECTION LENS_pHMPD_3DVIS_2008 (550nm)

FIG. 12D

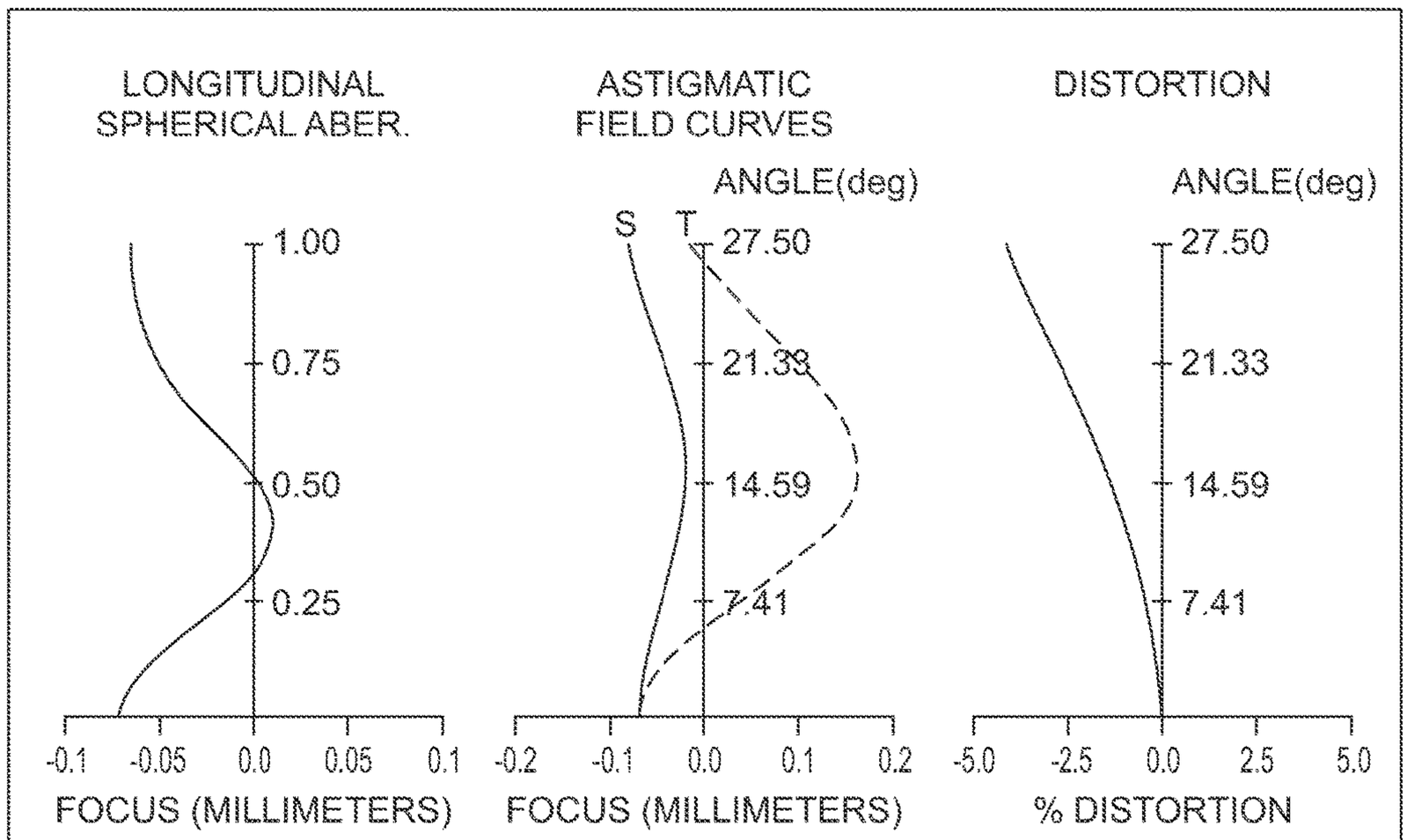
LONGITUDINAL
SPHERICAL ABER.
1.00
0.75
0.50
0.25
-0.1
-0.05
0.0
0.05
0.1
FOCUS (MILLIMETERS)
ASTIGMATIC
FIELD CURVES
ANGLE(deg)
S
T
27.50
21.33
14.59
7.41
-0.2
-0.1
0.0
0.1
0.2
FOCUS (MILLIMETERS)
DISTORTION
ANGLE(deg)
27.50
21.33
14.59
7.41
-5.0
-2.5
0.0
2.5
5.0
% DISTORTION
PROJECTION LENS_pHMPD_3DVIS_2008 (650nm)

FIG. 12E

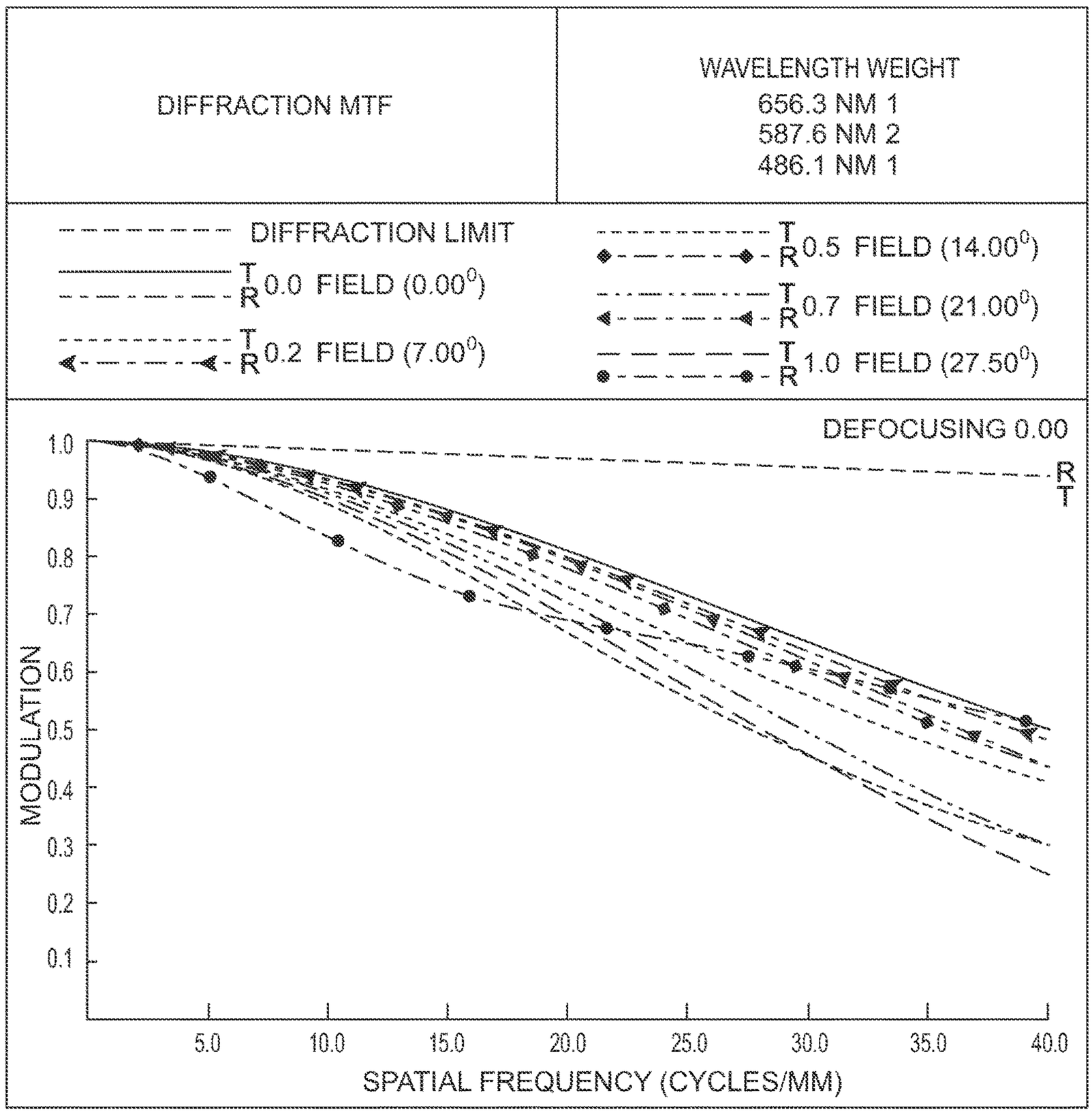
DIFFRACTION MTF
WAVELENGTH WEIGHT
656.3 NM 1
587.6 NM 2
486.1 NM 1
DIFFRACTION LIMIT
T R 0.0 FIELD (0.00°)
T R 0.2 FIELD (7.00°)
T R 0.5 FIELD (14.00°)
T R 0.7 FIELD (21.00°)
T R 1.0 FIELD (27.50°)
DEFOCUSING 0.00
R T
MODULATION
1.0
0.9
0.8
0.7
0.6
0.5
0.4
0.3
0.2
0.1
5.0
10.0
15.0
20.0
25.0
30.0
35.0
40.0
SPATIAL FREQUENCY (CYCLES/MM)

FIG. 12F

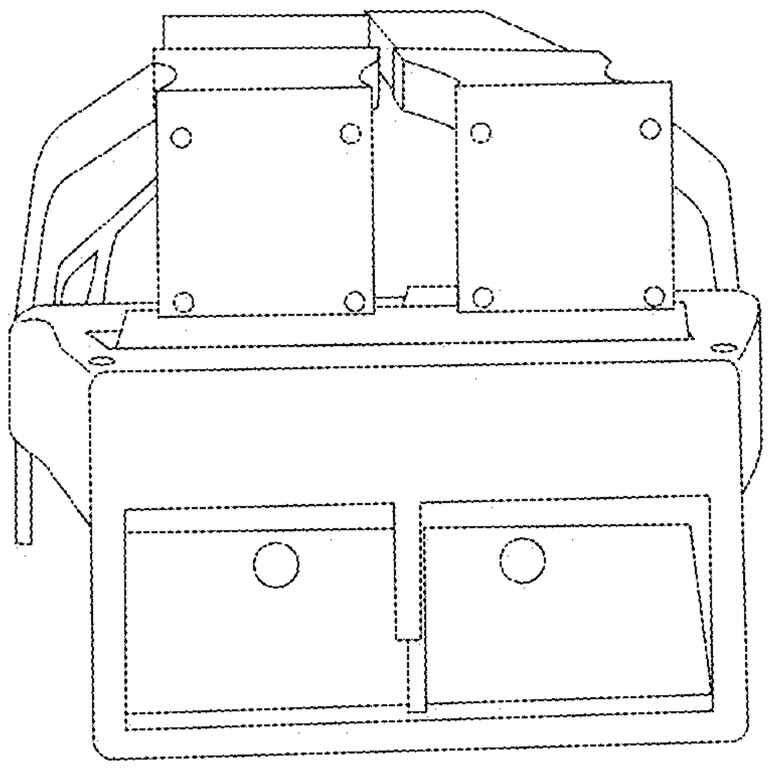

FIG. 13A

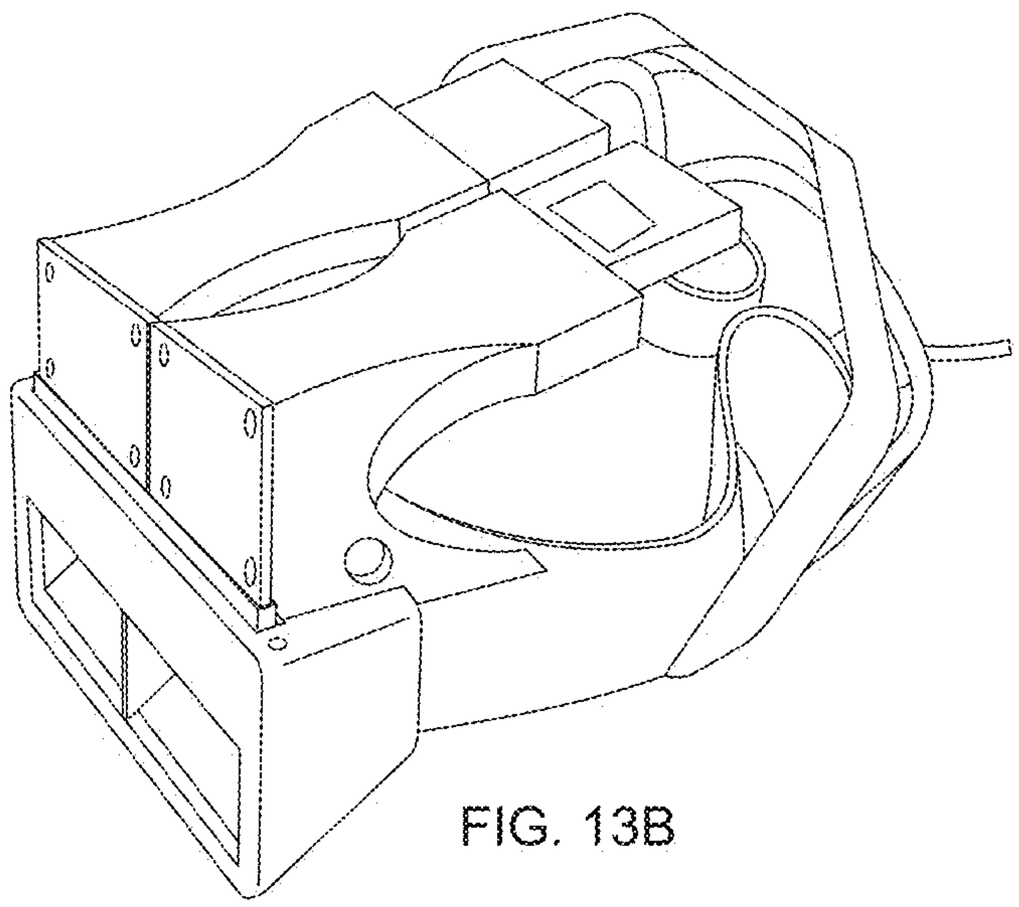

FIG. 13B

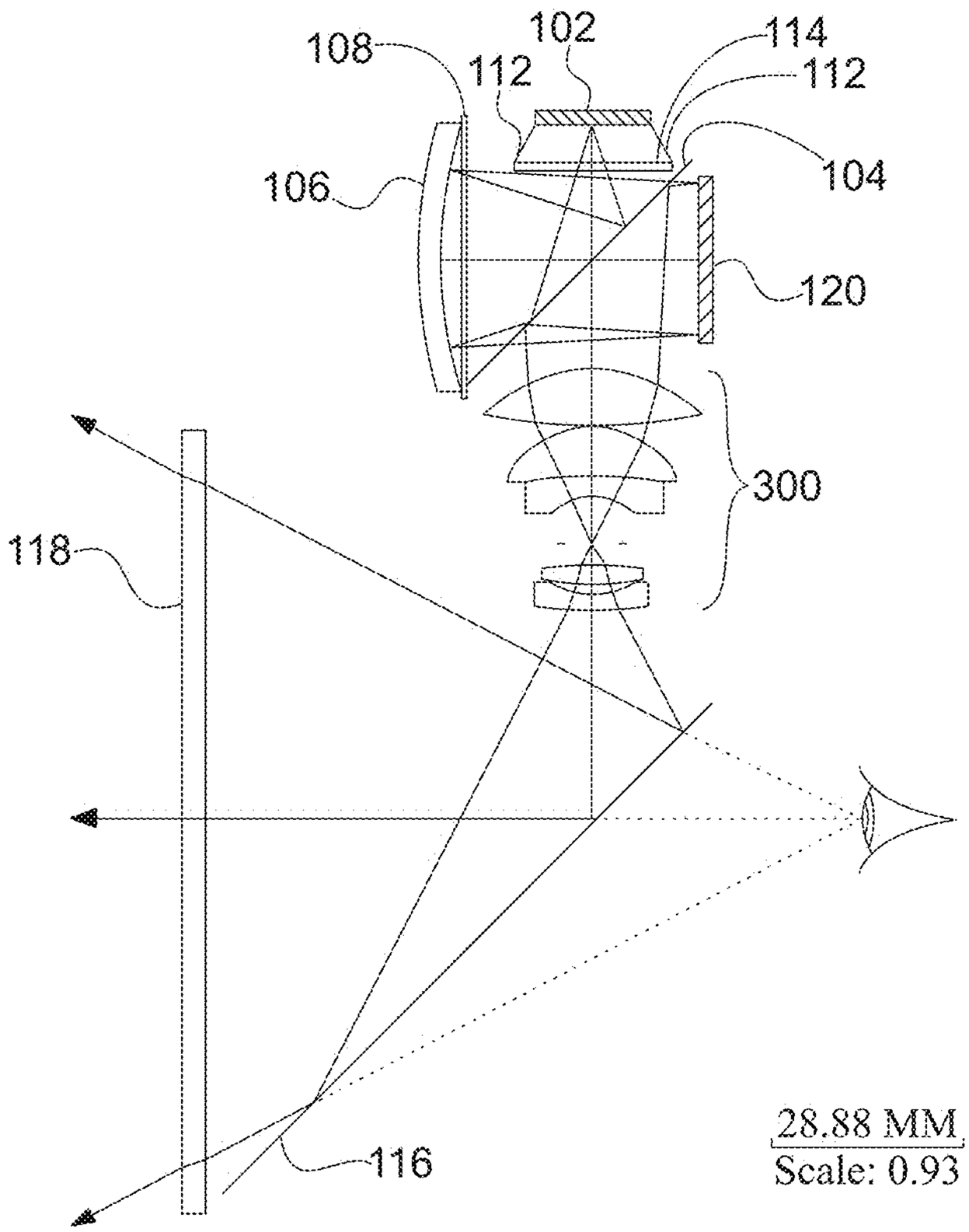

FIG. 14

HEAD-MOUNTED PROJECTION DISPLAY USING REFLECTIVE MICRODISPLAYS

RELATED APPLICATIONS

This application is a continuation application of U.S. application Ser. No. 13/955,076 filed on, Jul. 31, 2013, which is divisional application of U.S. application Ser. No. 12/863,771 filed on Oct. 29, 2010, which is a 371 application of International Application No. PCT/US2009/31606 filed Jan. 21, 2009, which claims the benefit of priority of U.S. Provisional Application No. 61/011,789, filed on Jan. 22, 2008, the entire contents of which applications are incorporated herein by reference.

GOVERNMENT RIGHTS

This invention was made with government support under government contract IIS0534777 awarded by the National Science Foundation. The government has certain rights in the invention.

FIELD OF THE INVENTION

The present invention relates generally to a head-mounted projection display, and more particularly, but not exclusively to a polarized head-mounted projection display including a light engine and a compact, high-performance projection lens for use with reflective microdisplays.

BACKGROUND OF THE INVENTION

The head mounted projection display (HMPD), as an alternative to the conventional eyepiece-based head mounted display (HMD), has attracted much interest in recent years, because it offers the ability to design a wide field of view (FOV), low distortion and ergonomically compact optical see-through head mounted display (OST-HMD). Like most OST-HMDs, however, one of the limiting factors for the HMPD technology is its low image brightness and contrast, which limits the feasibility to apply such information to outdoor or well-lit indoor environments such as operating rooms. Due to the multiple beamsplitting through a beamsplitter and low retroreflectivity of typical retroreflective materials, the overall efficiency of a HMPD is around 4%. For instance, with a miniature backlit active matrix liquid crystal display (AMLCD) as the image source, the luminance of the observed image is estimated to be 4 cd/m^2, while the average luminance of a well-lit indoor environment is over 100 cd/m^2. As a result, the low-brightness image of HMPDs will appear washed out in such well-lit environments. In fact, most optical see-through HMDs, including HMPD, are typically operated under a dimmed lighting condition.

To address this problem, a polarized head-mounted projection display (p-HMPD) was proposed (H. Hua and C. Gao, "A polarized head-mounted projective displays," *Proceedings of* 2005 *IEEE and ACM International Symposium on Mixed and Augmented Reality*, pp. 32-35, October 2005) and a prototype based on a pair of transmissive AMLCDs was designed recently (H. Hua, C. Gao "Design of a bright polarized head-mounted projection display" *Applied Optics*, Vol. 46, Issue 14, pp. 2600-2610, May 2007). A pair of 1.3" color AMLCDs was used as the image sources which have a resolution of (640*3)*480 pixels. 1.4" Alphalight™ RGB LED panels (Teledyne Inc., Los Angeles, Calif.) were used as the backlighting sources. By carefully manipulating the polarization states of the light propagating through the system, a p-HMPD can potentially be three times brighter than a traditional non-polarized HMPD design using the same microdisplay technologies. A schematic design of a monocular p-HMPD configuration is illustrated in FIG. **1**.

The image on the LCD display is projected through the projection lens, forming a real intermediate image. The light from the LCD is manipulated to be S-polarized so that its polarization direction is matched with the high-reflection axis of the polarized beamsplitter (PBS). After the projected light is reflected by the PBS, it is retroreflected back to the same PBS by a retroreflective screen. The depolarization effect by the retroreflective screen is less than 10% within ±20 degrees and is less than 20% up to ±30 degrees. As a result, the retroreflected light remains dominantly the same polarization as its incidence light. In order to achieve high transmission through the PBS after the light is retroreflected back, a quarter-wave retarder is placed between the PBS and the retroreflective screen. By passing through the quarter wave retarder twice, the incident S-polarized light is converted to P-polarization and transmits through the PBS with high efficiency. Thus the projected image from the microdisplay can be then observed at the exit pupil of the system where the eye is placed.

However, since a transmissive LCD microdisplay has a low transmission efficiency of around 5%, the overall performance of the first p-HMPD prototype is still unsatisfactory in a well-lit environment. Furthermore, owing to its inherent low pixel fill factor, a transmissive AMLCD microdisplay typically has a relatively low resolution. Accordingly, it would be an advance in the field of head-mounted projection displays to provide a head-mounted projection display which has higher luminance while maintaining high contrast.

SUMMARY OF THE INVENTION

In one of its aspects, the present invention provides a compact, telecentric projection lens for use in a head-mounted projection display system. The projection lens may include a plurality of lens elements configured to have an overall length that is no more than about two times the effective focal length of the projection lens. In addition, the plurality of lens elements may be configured so that the projection lens is telecentric in image space. As one measure of the compactness the projection lens may have an overall length that is no more than about 85% larger than the effective focal length of the projection lens. Further, the projection lens may have a back focal length that is about 40% larger than the effective focal length. To further facilitate the use of the projection lens in a head-mounted display, the projection lens may also be lightweight and have a ratio of the weight of the projection lens to the square of the F-number of the projection lens of less than about 2 to 1. For example, in one configuration the present invention provides a projection lens with a F-number of 2.1 and a weight of only 8.2 g.

In another of its aspects the present invention provides a telecentric optical illumination system for use with a reflective microdisplay. The illumination system may include a source of optical radiation having a first polarization state and a polarized beamsplitter disposed at a location to receive optical radiation from the optical radiation source. The beamsplitter may further be oriented relative to the source of optical radiation to reflect the received optical radiation. In addition, the illumination system may include an optical retarder disposed at a location relative to the beamsplitter to

receive optical radiation reflected by the beamsplitter and oriented to convert the polarization state of the received optical radiation to be circularly polarized. A reflector having optical power may also be disposed at a location to receive the circularly polarized optical radiation from the optical retarder and to reflect the received optical radiation back through the retarder and beamsplitter. The reflector may be a concave spherical reflector. Still further, in order to provide an optical illumination system that is telecentric in image space, the illumination system may include a pupil disposed at the source of optical radiation.

In yet another of its aspects, the present invention provides a head-mounted projection display system which may include the aforementioned illumination system, a microdisplay disposed one reflector focal length away from the reflector for receiving optical radiation from the reflector, and a telecentric projection lens. The projection lens may assume the configuration of the aforementioned projection lens.

BRIEF DESCRIPTION OF THE DRAWINGS

The foregoing summary and the following detailed description of the preferred embodiments of the present invention will be best understood when read in conjunction with the appended drawings, in which:

FIG. **1** schematically illustrates a polarized HMPD system comprising a transmissive AMLCD and retroreflection screen;

FIG. **2** illustrates the luminance distribution of an exemplary LED illuminator used in a light engine of the present invention;

FIG. **3** schematically illustrates an exemplary design of a light engine in accordance with the present invention;

FIG. **4** illustrates a prototype of a mirror based light pipe of the light engine of the present invention;

FIG. **5** schematically illustrates an exemplary design of the tapered light pipe of FIG. **4**;

FIGS. **6**A, **6**B illustrate the illuminance distribution on the microdisplay provided by the light engine of FIG. **3**, without and with light pipe, respectively;

FIG. **7** illustrates the layout of an initial lens used as a starting point in the design of a projection lens of the present invention;

FIGS. **8**A, **8**B illustrate a lens layout and MTF performance, respectively, for an optimized version of the lens of FIG. **7**;

FIGS. **9**A, **9**B illustrate a lens layout and MTF performance, respectively, for further optimized version of a projection lens of the present invention which is more compact than the lens of FIG. **8**;

FIG. **10** illustrates the layout of the final design of an exemplary projection lens of the present invention;

FIGS. **11**A, **11**B illustrate the diffraction efficiency versus radius and diffraction efficiency versus wavelength, respectively, for the projection lens of FIG. **10**;

FIGS. **12**A, **12**B illustrate a spot diagram and ray fan plot, respectively, for the projection lens of FIG. **10**;

FIGS. **12**C-**12**E illustrate the longitudinal spherical aberration, astigmatism, and distortion at 450 nm, 550 nm, 650 nm, respectively, for the projection lens of FIG. **10**;

FIG. **12**F illustrates the MTF performance for the projection lens of FIG. **10**;

FIGS. **13**A, **13**B illustrate a front view and a side perspective view, respectively, of a prototype of a polarized head-mounted projection display of the present invention; and

FIG. **14** schematically illustrates polarized head-mounted display in accordance with the present invention which includes the light engine of FIG. **3** and projection lens of FIG. **10**.

DETAILED DESCRIPTION

In order to realize the above-mentioned benefits afforded by a reflective microdisplay **120** in the context of a head-mounted projection display, suitable optical designs are required for both a light engine **100**, to deliver uniform, telecentric illumination to the microdisplay **120**, and for a telecentric projection lens **300** to collect the light reflected by the microdisplay **120** for delivery to the user, FIG. **3**. In addition to the requirements of telecentricity and uniformity, the light engine **100** and projection lens **300** must be sufficiently compact and lightweight to permit their use as part of the head-mounted system. In this regard, in one of its aspects, the present invention provides a compact, telecentric light engine **100** that includes a light pipe **110** and polarization manipulating components **104**, **108** to increase the overall uniformity and brightness, respectively, of the light delivered to a reflective microdisplay **120**, FIG. **3**. In another of its aspects, the present invention provides a telecentric projection lens **300** comprising all plastic components having aspheric surfaces and a diffractive optical element to yield a lens **300** that is simultaneously compact, telecentric, and lightweight, FIG. **10**. Together, the light engine **100**, reflective microdisplay **120**, and projection lens **300** provide a polarized HMPD in accordance with the present invention, FIG. **14**.

Turning now to the overall system, design began by selection of an exemplary microdisplay **120** from which the performance requirements of both the light engine **100** and projection lens **300** may be derived. Major properties of several candidate microdisplay technologies were evaluated, including AMLCD, organic light emitting displays (OLEDs), liquid crystal on silicon (LCOS), and ferroelectric Liquid-crystal-on-Silicon (FLCOS) were considered. For use in the examples provided below, the SXGA-R2D FLCOS microdisplay kit (Forth Dimensional Displays Limited, Birmingham, UK) was selected as an exemplary microdisplay for use in the present invention due to its high resolution, optical efficiency, and compactness. However, though a FLCOS microdisplay is used for illustrative purposes in the designs presented below, it is understood that the present invention is not limited to such a microdisplay, but may be used in conjunction with suitable other displays, such as, reflective microdisplay types like LCOS, MEMS, Texas Instruments DLP, and so forth, for example.

The usage of a FLCOS microdisplay **120** makes the prototype design of a HMPD quite different from previous designs of HMPD optics. One of the key differences is the requirement for the custom-designed light engine **100** to illuminate the microdisplay **120**. The FLCOS microdisplay **120** is considered as the combination of a mirror and an electrically switchable quarter-wave retarder formed by the liquid crystal layers. The FLCOS microdisplay **120** works most efficiently when the illumination rays are normally incident upon the display surface. To ensure the high contrast of the output image, it is recommended to limit the incident angle to the range of ±16 degrees, which imposes a critical requirement on the design of both the light engine **100** and projection lens **300**. The key requirements for the light engine **100** include: (1) that the illumination system be image-space telecentric to ensure that for every pixel on the

display surface the incident chief ray is normal to the display surface; and (2) that the cone angle of the ray bundle is smaller than 16 degrees.

Likewise, owing to the reflective nature of the microdisplay **120**, the output ray bundles from every pixel of the microdisplay **120** are telecentric with a cone angle smaller than 16 degrees. To efficiently collect rays from the microdisplay **120** and form a projected image with uniform illumination, the projection lens **300** must be image-space telecentric. To the contrary, a projection system using backlit AMLCDs, which have a relatively large viewing angle, and thus relaxed requirement for the angle of incidence ray bundles, can relax the telecentric constraint to gain compactness.

TABLE 1

Specification of microdisplay and LED panel

Parameters	Specifications
FLCOS microdisplay	
Diagonal Size	22.3 mm
Active area	17.43 × 13.95 mm
Resolution	1280 × 1024 pixels
Pixel size	13.6 μm
Color technique	Field sequential color
LED panel	
Body Dimensions	18.4 × 14.1 mm
Active area	8.4 × 6.5 mm
Weight	4 ± .5 grams
Luminance	34800 (cd/m^2)
Color Coordinates	Red: x = .67-.43, y = .27-.33
	Green: x = .14-.28, y = .64-.73
	Blue: x = .11-.15, y = .04-.10
Power	340 mW

Design of a Compact Light Engine

Light source selection is the first step in the light engine design. Based on the design requirement of a HMPD, there are several constraints on the source selection and the light engine design. First, safety is a primary concern in any head-mounted device. Therefore sources with low power consumption and low heat dissipation are highly desired. Secondly, compactness and low weight are always critical for HMD systems. Finally, in order to generate an image with high brightness and uniformity across the whole FOV, the illumination on the microdisplay **120** should be uniform and bright. A 0.5" Alphalight color LED panel **102** (Teledyne Inc., Los Angeles, Calif.) is selected for the p-HMPD prototype design. The LED panel **102** is compatibly driven by the color sequential technique of the FLCOS displays. Table 1 summarizes the major specifications of the microdisplay **120** and LED panel **102**. The luminance distribution of the LED panel **102**, FIG. **2**, is relatively uniform within 18 degrees of the emitting angle. With the requirement of image-space telecentricity on the light engine **100**, a compact light engine design in accordance with the present invention is shown in FIG. **3**.

The basic idea of the design of the light engine **100** is to place the LED panel **102** at the front focal point of a positive lens (or reflector) and the microdisplay **120** at the back focal point. In order to make a compact system, a concave spherical reflector **106**, a PBS **104** and a quarter wave retarder **108** are used to fold the length of the system in half. The microdisplay **120** is disposed at the conjugate position of the LED panel **102**, and both the microdisplay **120** and LED panel **102** are at the focal point of the reflector **106**. With a polarizer **114** in front of the LED panel **102**, S-polarized light from the LED panel **102** is transmitted through the polarizer **114** and is reflected by the PBS **104**. A quarter-wave retarder **108** is placed between the reflector **106** and PBS **104** and its fast axis is at 45 degrees with the polarization direction of S-polarized light. By passing through the retarder **108** twice, the reflected light by the reflector **106** becomes P-polarized light and will transmit the PBS **104** to illuminate the microdisplay **120** with high efficiency.

In this design, the LED panel **102** itself can be taken as the pupil of the system to form an image-space telecentric system, where the ray bundle received by the microdisplay **120** is symmetric with the display normal. With both LED panel **102** and microdisplay **120** at the focal point of the reflector **106**, the light distribution on the microdisplay **120** is the Fourier transform of that of the LED panel **102**. Thus the spatial distribution on the microdisplay **120** can be derived as

$$E_{display}(x, y) = L * \Omega = L_{LED}\left(\arctan\left(\frac{\sqrt{x^2 + y^2}}{f}\right)\right) * \frac{S_{LED}}{f^2}. \quad (1)$$

where $E_{display}(x,y)$ is the illuminance at (x,y) on the display assuming the center of the display is at the origin, $L_{LED}(\theta)$ is the luminance of LED panel **102** as a function of angle, S_{LED} is the area of the LED panel **102** and f is the focal length of the reflector **106**. Across the microdisplay **120**, the ratio of the luminance at the center of the microdisplay **120** to that at the edge is

$$L_{LED}(0^\circ) \Big/ L_{LED}\left(\arctan\left(\frac{D}{2f}\right)\right)$$

while D is the diagonal size of the microdisplay **120**. To get better uniformity on the microdisplay **120**, a reflector **106** with larger focal length is preferred. But meanwhile, larger focal length will result in a less compact structure and a smaller solid angle with lower luminance efficiency. Considering all these factors, a reflector **106** with 35 mm focal length and 35 mm diameter was selected. As a result, the ratio of the maximum luminance to the minimum luminance on the microdisplay **120** is 1:0.82, and the cone angle of the ray bundle on the microdisplay **120** is within 8.6 degrees. The light within the cone angle of 18 degrees emitted by the LED panel **102** can be collected by the reflector **106** to illuminate the microdisplay **120** while the light emitted at a larger angle is wasted.

In order to further improve the light efficiency and uniformity of the light engine **100**, a mirror-based tapered light pipe **110** was designed to recycle the light with emission angles larger than 18 degrees. FIG. **4** shows a prototype design of the light pipe **110**. It is composed of four mirrors **112**, each of which is tilted by an angle with respect to the LED surface, forming a truncated pyramid shape. The light emitted from the LED panel **102** with large angles will be reflected by the enclosing mirrors **112**. After reflection, more rays from LED panel **102** can be collected by the reflector **106** to illuminate the microdisplay **120**. To get the best performance of the light engine **100**, both tilt angle, α, and length, t, of the light pipe mirror **112**, as shown in FIG. **5**, should be optimized.

Numerical Simulation

To determine the parameters of the tapered light pipe **110** and to examine the light efficiency and uniformity of the light engine **100**, the light engine **100** was modeled using LightTools® (Optical Research Associates, Pasadena, Calif.). In the simulation, the total power of the source was set to be 1 lumen. A light receiver was placed on the microdisplay **120** to estimate the efficiency of the light engine **100** and to evaluate the light distribution on the microdisplay **120**. Through the simulation, it is shown that the light engine **100** has higher uniformity and light efficiency when the tilt angle, α, of the mirror is 18 degrees. By balancing the performance and space constraint of the light engine **100**, the mirror length, t, is selected to be 8 mm. FIG. **6**B shows the output illuminance distribution on the microdisplay **120** for a system with the mirror based light pipe **110**, and FIG. **6**A shows the output illuminance distribution on the microdisplay **120** for the same system as FIG. **6**B but without the light pipe mirrors **112** in place. Hence, comparison between FIGS. **6**A, **6**B illustrates the improvement in performance of the light engine **100** due to the presence of the light pipe mirrors **112**.

As indicated by the simulation results, with a mirror based light pipe **110**, the light efficiency has increased from 8.93% to 12.3%, and the non-uniformity, quantified by the average standard deviation of the illuminance distribution across the display area, has reduced from 5.61% to 2.15%. Thus, the system with the light pipe **110** has higher efficiency and better uniformity than without.

Design of a Compact, High-Performance Projection Lens

Based on the design of the light engine **100**, a lightweight and compact image-telecentric projection lens **300** is designed. In this section, the design process of the projection lens **300** is described and the performance of the projection lens **300** is analyzed.

TABLE 2

Design targets for the projection lens

Parameter	Specification
Effective focal length	21.6 mm
Entrance pupil	10 mm
Image mode	Image space telecentric
OAL	<40 mm
OAL/BFL	<1.85
BFL	30.5 mm
FOV	55°
Wavelength range	486-656 nm
Distortion	<4% over FOV
Weight	<15-20 grams

Projection Lens Specification

Although projection optics do not scale as much with the increase of FOV as eyepiece-type optics, which makes designing wide FOV, optical see-through HMPD systems relatively easier than conventional HMDs, there are a few factors in HMPD systems that impose limits on the FOV. First of all, the use of a planar PBS **116** or a regular beamsplitter in front of the eye, which is oriented at 45 degrees with the optical axis, sets up the FOV upper limit of 90 degrees. Furthermore, a wide FOV requires a large size of PBS **116** and retarder **118** and consequently challenges the compactness and lightweight of the display system. The limit of allowable PBS and retarder dimensions is set by the interpupilary distance (IPD), which is in the range of 55 to 75 mm for over 95% of the population. Thirdly, previous investigation on retroreflective materials shows that the retroreflectance of currently available materials drops off significantly for light incident at angles beyond ±35°. A FOV beyond 70 degrees will inevitably cause vignetting-like effect and compromise image uniformity. Finally, the angular resolution of the microdisplay **120** degrades with the increase of the FOV. Taking into account these factors, a target was set to design the projection system with a FOV of 55 degrees, which corresponds to an effective focal length (EFL) of 21.6 mm for the selected FLCOS microdisplay **120**.

In addition to being image-space telecentric, the projection lens **300** must have a large back focal length (BFL) to ensure enough space for the PBS **104** which is placed between the microdisplay **120** and projection lens **300**. Based on the light engine design, the BFL is chosen to be at least 30.5 mm. Thus this projection lens **300** is also a reverse telephoto lens. (It is understood that, in the designs below, the microdisplay **120** is located at the image plane, hence the reason that the BFL represents the space allotted for the PBS **104** placed therebetween.)

Since a user's eye is positioned at the conjugate position to the entrance pupil of the projection lens **300**, the entrance pupil diameter is very critical for comfortable observation. Typically it is suggested the pupil diameter of the projection system for HMPDs should be around 10-12 mm. This range of pupil size allows an eye swivel of about ±21° up to 26.5° within the eye sockets without causing vignetting or loss of image with a typical 3-mm eye pupil in the lighting conditions provided by HMPDs. Furthermore, it allows a ±5 mm to 6 mm IPD tolerance for different users without the need to mechanically adjust the IPD of the binocular optics. Considering the short focal length of the optics, a target entrance pupil with a diameter of at least 10 mm was selected, which leads to a projection system with an F/# of 2.16.

A lens 10 from Nanba U.S. Pat. No. 6,236,521 was used as the starting point of the design, with FIG. **7** showing the layout. The starting lens 10 was designed for a digital projector, and is reverse-telephoto and telecentric. Unlike a double Gauss lens, the starting lens **10** has an asymmetric structure relative to the stop because of the telecentric requirement in image space. This five-element starting lens **10** offers a full FOV of 65 degrees with an F/# of 2.5. Among the five glass elements, a doublet **12** is used, and the front surface **14** of the last element **16** is aspheric to help correct spherical aberration. The ratio of the BFL to the EFL of the lens **10** is 1.13 and the ratio of the overall length (OAL. As used herein, OAL refers to the distance from the first surface of the first optical element to the last surface of the last optical element) of the optics to the EFL is 3.15. The ratio of the exit pupil distance to the EFL is 13.6, which makes the lens **10** telecentric in image space. By scaling and several cycles of optimization with CODE V® (Optical Research Associates, Pasadena, Calif.), a new starting lens **210** was obtained to meet the first-order design targets of 21.1 mm EFL, 30 mm BFL and 68 mm OAL, as shown in FIG. **8**A and Table 3. The full FOV is set to be 55 degrees. As shown in FIG. **8**B, the MTF of the lens **210** is around 30% at the spatial frequency of 37-lp/mm, which shows acceptable performance as a first-order starting point for the design.

TABLE 3

Numerical values for lens of FIG. 8.

Surface No.	Surface type	Radius	Thickness	Lens material
1	Sphere	151.9831514	7.199	772499.496
2	Sphere	18.31108732	18.74851	
3	Sphere	37.26417226	4.646097	772499.496
4	Sphere	51.05918244	9.065786	
stop	Sphere	1.00E+18	11.41511	
6	Sphere	14.31228599	4.642326	846660.238
7	Sphere	121.7152043	6.393417	677900.553
8	Sphere	20.60785676	0.1	
9	Asphere	60.8179454	5.789755	772499.496
10	Sphere	38.94828517	29.99994	

Asphere parameters for surface 9
4th Order Coefficient (A) −8.95E−06
6th Order Coefficient (B) 6.83E−09
8th Order Coefficient (C) −1.56E−11
10th Order Coefficient (D) 2.28E−14

The projection lens **210** is rotationally symmetric, and thus the optimization is only necessary over half of the full FOV for the radial direction. Three representative wavelengths (i.e., 486 nm, 589 nm and 656 nm) were set with the weights of 1, 2 and 1, respectively. Five fields, corresponding to 0, 7°, 14°, 21° and 27.5°, respectively, were used in the optimization process to represent the half FOV. The weights of the five fields were adjusted in the optimization process to balance the MTF performances across the entire FOV. During the optimization, all surface curvatures, surface thicknesses, and coefficients of aspheric surfaces were set to be variables. Several constraints were set to satisfy the specifications of the overall system and each individual lens element, including the EFL, BFL, OAL, distortion requirements, and the center thickness of individual elements, for example. The telecentric requirement was satisfied by setting the exit pupil distance to be at least 210 mm from the image plane. This distance corresponds to a deviation of the chief ray by 3° from a perfectly telecentric system, which yields a good balance between the overall optical performance and the system compactness considering the difficulty in designing a perfectly telecentric lens with a short OAL.

One of the major problems of the lens **210** in FIG. **8**A is its compactness: the OAL is too large for a head-mounted system and a more compact solution is needed. This initial lens **210** was gradually optimized by adjusting the parameter constraints and field weights through a local optimization approach. While the OAL was reduced down to about 40 mm in the process of optimization, the overall performance was degraded as well. In order to further improve its performance, the back surface **211** of the first lens element **212** was set to be aspheric, which helped to correct most of the spherical aberration. After gradual optimization, a system was obtained with satisfactory performance. The resulting lens layout and MTF are shown in FIGS. **9**A, **9**B.

This lens **220** is composed of five glass elements **221-225** (with aspheres on two surfaces **227**, **229**) and weighs about 38.7 grams, which needs to be significantly reduced to obtain a lightweight p-HMPD system. Plastic materials were selected to replace the glass elements **221-225**. Considering that the density of glass is about three times of most plastics, it is expected that the weight of the lens **220** would drop to around 10 grams. The drawback of using the plastic materials is also obvious. While there are many choices of optical glass, from low to high refractive index and low to high Abbe number, for plastics only very limited number of materials are available for diamond turning fabrication.

The initial target was to replace the glass elements **223-225** on the right side of the stop with the plastics, since they contributed most of the weight due to their large aperture. Polystyrene with low Abbe number and Cyclic Olefin Polymer (COC) with relatively high Abbe number were selected to replace the glass materials of the doublet **223**, **224**. After this replacement, the optimization was rerun to achieve the desired specifications of the lens **220**. Since the last element **225** has the highest optical power among all the elements in the lens **220** and high Abbe number, COC was selected for the last element **225**. Unfortunately, after the plastic replacement the system had much worse performance compared with the system before replacing the last glass element **225**. Chromatic aberration dominates the resulting system. To effectively correct the residual chromatic aberration, a diffractive optical element (DOE) was added to the system.

A DOE can be viewed as a material with large dispersion but opposite in sign to conventional materials, i.e., the Abbe number of a DOE is approximately −3.5 for the visible spectrum. This DOE with negative Abbe number would help to correct the chromatic aberration. The substrate shape of a diffractive surface DOE can be spherical, planar being a special case, or aspheric. The commonly used orders of diffraction are 0, −1, or 1. The +1 order of diffraction was adopted. The diffractive surface can be used on any of the lens surfaces as long as it can help to correct the chromatic aberration. However, after a few trials, it was found to be most effective to place the diffractive surface on the left surface **227** of the last element **225**. The DOE quadratic coefficient was set to be a variable up to 12 orders in the optimization process. Finally, to further reduce the lens weight, the first two glass elements **221**, **222** on the left of the stop were replaced with Acrylic and Polystyrene, respectively.

Considering the fact that a doublet requires higher cost in the fabrication process, the doublet **223**, **224** was split into two single elements. The split of the doublet **223**, **224** also offered extra freedom in the optimization, and helped improve the overall performance. Finally, through several rounds of optimization, a telecentric lens **300** with an OAL of 34 mm and a total weight of 8.2 grams was obtained. The ratio of the weight of the lens to the square of the F-number was 1.86 to 1. FIG. **10** shows the layout of the final design of the projection lens **300**, and Tables 4-9 shows the design parameters and first order properties of the lens **300**.

TABLE 4

Numerical values for the lens of FIG. 10.

Surface No.	Surface type	Radius	Thickness	Material
1	Sphere	54.31648697	2	Acrylic
2	Asphere	11.67695001	1.31979	
3	Sphere	29.18891338	2.71793	Polystyrene
4	Sphere	−53.75253258	3.106908	
5(stop)	Sphere	Infinity	6.769705	
6	Asphere	−9.34878697	2.5	Polystyrene
7	Sphere	−109.22569406	0.2	
8	Sphere	−93.99209709	7.088732	Cyclic Olefin Polymer
9	Sphere	−14.34048220	0.1	
10	Asphere	36.51968881	8.196935	Cyclic Olefin Polymer
11	Sphere	−22.22836849	30.5	
image	Sphere	Infinity	0	

TABLE 5

Numerical values for aspheric surfaces of the lens of FIG. 10.

Element	Focal length (mm)
1st element	−30.7666976612
2nd element	32.4497012224
First two elements	−7837.900440744
3rd element	−17.48717528244
4th element	30.96961073305
5th element	25.97749355667

TABLE 6

Numerical values for aspheric surfaces of the lens of FIG. 10.

Surface	Surface 2	Surface 6	Surface 10
Conic Constant (K)	1.19517273E+00	2.87739760E−01	−1.73713081E+01
4th Order Coefficient (A)	−9.17398530E−05	1.55078027E−04	1.87808847E−07
6th Order Coefficient (B)	−6.00685014E−06	1.60075455E−06	−1.36998214E−07
8th Order Coefficient (C)	2.67960130E−07	−1.10443177E−07	7.55859302E−10
10th Order Coefficient (D)	−9.29841239E−09	4.67064799E−09	−2.04509691E−12
12th Order Coefficient (E)	1.54727549E−10	−8.56490951E−11	2.26702680E−15
14th Order Coefficient (F)	−1.16675172E−12	6.81530567E−13	−1.54585020E−19

TABLE 7

Numerical values for the DOE of the lens of FIG. 10.
Diffraction Order = 2
Construction Wavelength = 550

R**2 (C1)	−1.06653506E−03
R**4 (C2)	4.09441040E−06
R**6 (C3)	−4.17021652E−08
R**8 (C4)	2.36559269E−10
R**10 (C5)	−6.59579639E−13
R**12 (C6)	7.29317846E−16

TABLE 8

Numerical values for optical materials of the lens of FIG. 10.

	Acrylic	Polystyrene	Cyclic Olefin Polymer
Trade Name	Plexiglas	Styron	Zeonex
nf (486.1 nm)	1.497	1.604	1.537
nd (589 nm)	1.491	1.590	1.530
nc (656.3 nm)	1.489	1.585	1.527

TABLE 9

First order properties of the lens of FIG. 10 at infinite conjugates.

EFL	21.6000
BFL	30.5000
FFL	4.5965
F No	2.1600
Image distance	30.5000
OAL	34.0000
Paraxial image height	11.2442
Paraxial image Ang	27.5000
Ent pupil diameter	10.0000
Ent pupil thickness	7.0384
Exit pupil diameter	88.4570
Exit pupil thickness	−160.5672

The lens **300** includes five lens elements **310**, **320**, **330**, **340**, **350** ordered left-to-right from object space to image space. The first two lens elements **310**, **320** form a first lens group **315** having very little optical power (e.g., the focal length of the lens group **315** is two orders of magnitude larger than that of the lens **300**, see Tables 5, 9) disposed to the left of the stop. The first lens element **310** is a negative meniscus lens having two surfaces that are concave towards image space, with the surface **311** closest to image space being aspheric. The second lens element **320** is a positive lens disposed adjacent the first lens element **310**. The third through fifth lens elements **330**, **340**, **350** are disposed on the right side of the stop, with the third element **330** closest to the stop being a negative lens and the fourth and fifth elements **340**, **350** closest to the image plane being positive lenses. The first surface **331** of the third lens element **330** closest to the stop is aspheric as is the first surface **351** of the fifth lens element **350**. In addition, the first surface **351** of the fifth lens element **350** includes the aforementioned DOE.

Performance Analysis of the Projection Lens

The diffraction efficiency of a DOE drops as its physical features become finer near the edge. FIG. **11**A shows the diffraction efficiency as a function of the radius of diffractive surface at the designed wavelength 550 nm. The overall efficiency varies from 98.7% at the center to 98.5% at the edge. The diffraction efficiency is also wavelength dependent. FIG. **11**B plots the diffraction efficiency as a function of wavelengths as well as the levels of the binary masks (i.e., 2, 4, 8, 16). Level 16 could be an accurate prediction for the Kinoform DOE using diamond turning method for fabrication. It shows that the diffraction efficiency varies from 80% to 100% across the visible spectrum.

The optical performance of the optimized lens **300** is assessed on the image plane at the five representative field angles for three different wavelengths. The spot diagrams are shown in FIG. **12**A. The average RMS spot diameter across the FOV is around 16 μm, which is slightly larger than the 13.6 μm pixel size to avoid pixellated artifacts. FIGS. **12**C-E shows longitudinal spherical aberration, astigmatism, and the distortion curves. The longitudinal spherical aberration and astigmatism are well balanced, and the distortion of the system is limited within 4% across the FOV. The MTF of the lens **300** is presented in FIG. **12**F. The FLCOS microdisplay **120** has a threshold spatial frequency of 36.8-lp/mm given a 13.6 μm pixel size (i.e. threshold spatial frequency=1/(2*pixel size)). The modulation is about 40% at 36.8-lp/mm across the whole FOV, which means the performance of the system is currently limited by the display resolution.

p-HMPD Prototype

With the design of the light engine **100** and projection lens **300** complete, a prototype of the new p-HMPD was built, FIGS. **13-14**. The p-HMPD included the light engine **100**,

microdisplay **120**, and projection lens **300**, as well as an additional PBS **116**, quarter-wave retarder **118**, and retro-reflective screen, which are disposed in the same relative positions to provide the same function as the PBS, quarter-wave retarder, and retro-reflective screen of FIG. **1**. Compared with the p-HMPD prototype using transmissive LCD microdisplays of FIG. **1**, the mounting of the optics in the new p-HMPD of FIG. **3** is more challenging for the following reasons. First, the use of the light engine **100** requires some extra space and weight. Second, the projection lens **300** designed for the FLCOS microdisplay **120** is longer due to the image-space telecentric requirement and higher image quality requirement.

Considering both the ergonomic and aesthetic factors, the optics **100**, **120**, **300**, were mounted vertically so that the width of the helmet was around the average width of the adult head. In the vertical direction, the optics were mounted according to the shape of the head, and the associated electronics were mounted on the top of the helmet. A main drawback of the vertical mount is that a ghost image of the ground formed by the PBS **104** is overlaid with the projected image, which leads to reduced image contrast. This problem, however, can be solved by blocking the optical path from the ground.

To make the system more compact and lighter, the mount of the light engine **100** with the microdisplays **120** was fabricated separately and then integrated with the shell as a whole. The lens **300** position relative to the microdisplay **120** is adjustable to provide a projected image with adjustable magnification.

The helmet shells were fabricated using rapid prototyping techniques, in which physical models are fabricated layer by layer directly from a 3D CAD model. The helmet shells were assembled and attached to an off-the-shelf headband that offers head-size adjustment. The front and side views of the prototype are shown in FIGS. **13**A, **13**B, respectively.

These and other advantages of the present invention will be apparent to those skilled in the art from the foregoing specification. Accordingly, it will be recognized by those skilled in the art that changes or modifications may be made to the above-described embodiments without departing from the broad inventive concepts of the invention. It should therefore be understood that this invention is not limited to the particular embodiments described herein, but is intended to include all changes and modifications that are within the scope and spirit of the invention as set forth in the claims.

What is claimed is:

1. A head-mounted projection display system, comprising:

a microdisplay comprising a plurality of pixels;

an illumination system and a projection system having a chief ray and a ray bundle, each system in optical communication with one another and with the microdisplay and each system telecentric in image space relative to the microdisplay such that the chief ray incident at the surface of the microdisplay is normal to the surface and the cone angle of the ray bundle is less than 16°.

2. The head-mounted projection display system according to claim **1**, wherein the microdisplay is reflective, and the bundle of rays is reflected from the microdisplay to be telecentric with the cone angle smaller than 16°.

3. The head-mounted projection display system according to claim **2**, wherein the incident chief ray is normal to the microdisplay surface at each pixel of the microdisplay.

4. The head-mounted projection display system according to claim **1**, wherein the incident chief ray is normal to the microdisplay surface at each pixel of the microdisplay.

5. The head-mounted projection display system according to claim **1**, wherein the cone angle of the ray bundle is less than 9°.

6. The head-mounted projection display system according to claim **1**, wherein the illumination system comprises a light engine.

7. The head-mounted projection display system according to claim **6**, wherein the light engine comprises a mirror-based tapered light pipe.

8. The head-mounted projection display system according to claim **1**, wherein the illumination system includes a light source and the projection system includes a front focal point and a back focal point, and wherein the light source is disposed at the front focal point and the microdisplay is disposed at the back focal point.

9. The head-mounted projection display system according to claim **8**, wherein the microdisplay is disposed at a conjugate position to the light source.

10. The head-mounted projection display system according to claim **1**, comprising a reflector having optical power, a beam splitter, and quarter wave retarder each disposed in between the illumination system and the microdisplay.

11. The head-mounted projection display system according to claim **10**, wherein the microdisplay and a light source of the illumination system are disposed at a focal point of the reflector.

* * * * *